

A TIDAL DISRUPTION FLARE IN ABELL 1689 FROM AN ARCHIVAL X-RAY SURVEY OF GALAXY CLUSTERS

W. PETER MAKSYM AND M. P. ULMER

Department of Physics and Astronomy, Northwestern University, Evanston, IL 60208-2900

MICHAEL ERACLEOUS

Department of Astronomy and Astrophysics and Center for Gravitation Wave Physics,
 The Pennsylvania State University, 525 Davey Lab, University Park, PA 16803

Draft version August 23, 2008, accepted for publication in the Astrophysical Journal

ABSTRACT

Theory suggests that a star making a close passage by a supermassive black hole at the center of a galaxy can under most circumstances be expected to emit a giant flare of radiation as it is disrupted and a portion of the resulting stream of shock-heated stellar debris falls back onto the black hole itself. We examine the first results of an ongoing archival survey of galaxy clusters using *Chandra* and *XMM-Newton*-selected data, and report a likely tidal disruption flare from SDSS J131122.15-012345.6 in Abell 1689. The flare is observed to vary by a factor of $\gtrsim 30$ over at least 2 years, to have maximum $L_X(0.3 - 3.0 \text{ keV}) \gtrsim 5 \times 10^{42} \text{ erg s}^{-1}$ and to emit as a blackbody with $kT \sim 0.12 \text{ keV}$. From the galaxy population as determined by existing studies of the cluster, we estimate a tidal disruption rate of $1.2 \times 10^{-4} \text{ galaxy}^{-1} \text{ year}^{-1}$ if we assume a contribution to the observable rate from galaxies whose range of luminosities corresponds to a central black hole mass (M_\bullet) between 10^6 and $10^8 M_\odot$.

Subject headings: X-rays — Galaxies: X-rays — bursts, Galaxies: clusters: individual: A1689, Galaxies: Active, Galaxies: Nuclei — X-rays

1. INTRODUCTION

It is now generally accepted that massive black holes (MBHs) reside at the centers of massive galaxies (Magorrian et al. 1998). These central massive ($\geq 10^6 M_\odot$) black holes are expected to play an integral role in the formation and evolution of galaxies, but many uncertainties remain in this picture.

The low-mass cutoff for the central black hole mass spectrum is unknown and the population is inferred from the empirical relationship between MBHs and their host spheroid's velocity dispersion and associated luminosity (e.g., Magorrian et al. 1998; Marconi & Hunt 2003; Lauer et al. 2007) or AGN-based models of growth by accretion (Marconi et al. 2004). While some dwarf galaxies appear to host MBHs and are classified as AGNs, the active fraction decreases with decreasing mass and many common assumptions regarding the black hole distribution with respect to galaxy mass break down at lower M_\bullet (Greene et al. 2008). Indeed, an unknown fraction of dwarf galaxies may host no MBH at all but merely a nuclear stellar cluster (e.g. Ferrarese et al. 2006).

Outside of observations of the Galactic center (Ghez et al. 2003; Genzel et al. 2003), direct evidence of central black holes in the form of accretion events in non-AGN (normal) galaxies has been sparse. The most direct observational evidence of accretion events takes the form of flares produced by a star that passes close to the central black hole (Rees 1988). The passage is so close that the star is disrupted by the tidal forces it experiences. In this case, $\gtrsim 1/2$ of its mass is expelled into space as the remainder falls back to accrete onto the

black hole (Khokhlov & Melia 1996). Although much theoretical work has been done to describe the expected evolution of the debris and behavior of the resulting flare from an analytical (Loeb & Ulmer 1997; Ulmer 1999, e.g.) or numerical approach (Evans & Kochanek 1989; Khokhlov et al. 1993; Ayal et al. 2000; Bogdanović et al. 2004; Strubbe & Quataert 2009), on the order of a dozen solid observational examples have been so classified to date. See Gezari et al. (2009) for an summary of observations and (Alexander 2005) for a review of the theory.

Almost all the observations of tidal flares (or flare candidates) have been found in surveys of the field (Esquej et al. 2007, 2008; Donley et al. 2002) or in the UV (Gezari et al. 2009, 2006), and while our work was already in progress has there been an event reported to take place in a cluster of galaxies (Cappelluti et al. 2009).

Our paper is the first in a planned series of studies aimed specifically at monitoring clusters of galaxies for flares using archival *Chandra* and *XMM-Newton* data. This paper is based on observations of the first cluster we have chosen to study, Abell 1689 (Luminosity distance modulus 39.68, $z = 0.183^1$). Abell 1689 was an ideal choice for this survey because it exhibits many characteristics which maximized the chance of observing tidal flares given existing rate predictions.

Abell 1689 is among the richest of the Abell clusters, one of only 9 that has a richness of 4 or higher (Abell 665 is the only cluster of richness 5). At a redshift of

¹ From the NASA/IPAC Extragalactic Database (NED) which is operated by the Jet Propulsion Laboratory, California Institute of Technology, under contract with the National Aeronautics and Space Administration.

$z \sim 0.18$, with a virial radius r_{200} of $1.13 h^{-1}$ Mpc and hence about $10'$, the entire core of the cluster fits within a single *Chandra* ACIS chip (Andersson & Madejski 2004). Its richness has made it popular for examinations of the Sunyaev-Zeldovich effect, structure analysis, and lensing studies so it is well-observed in X-rays, optical and other wavelengths (e.g. Hubble) and hence an ideal starting point for our survey. With this extensive coverage (described in detail below) of a rich cluster of galaxies whose members are all effectively at the same redshift, we have thus been able to estimate the rate at which the galaxies experience tidal flare events.

In this paper we present the discovery of a transient event that we demonstrate to be most probably due to emission from a tidal flare and whose temperature is arguably the highest yet observed. For, although the derived peak observed flare temperature matches the highest reported peak blackbody temperature Cappelluti et al. (2009), our result was based on data from an instrument that provides about ~ 3 times better energy resolution than was used to derive the temperature of the Cappelluti et al. (2009) flare.

Furthermore, by monitoring so many galaxies in the field of view (FOV) at the same time, it was possible for us to set a limit to the frequency of flare events in a well defined galaxy population. Depending on the hypothesized event rate (e.g., Wang & Merritt 2004; Merritt 2009), our results may be used to delimit either the event rate or the very existence of massive black holes in dwarf galaxies. Tighter constraints on the event rate, as derived from the work presented here, are also interesting for predictions of event rates of the *Light Interferometer Space Antenna*² (hereafter *LISA*) which will be sensitive in the mass range of $M_{\bullet} \lesssim 10^7 M_{\odot}$ (Jennrich 2004; Sesana et al. 2004, 2005; Sigurdsson 2003; Kobayashi et al. 2004).

Throughout this paper, we adopt concordant cosmological parameters of $H_0 = 70 \text{ km s}^{-1} \text{ Mpc}^{-1}$, $\Omega_{m,0}=0.3$ and $\Omega_{\lambda,0}=0.7$, and calculate distances using Wright (2006). All coordinates are J2000. The galactic column density of neutral hydrogen for Abell 1689 is $1.82 \times 10^{20} \text{ cm}^{-2}$, derived using Dickey & Lockman (1990) values from the *colden* tool in *CIAO* (Fruscione et al. 2006) unless otherwise stated. All X-ray fluxes and luminosities used in this paper have been corrected for Galactic absorption using these values.

2. OBSERVATIONS AND DATA

2.1. Overview

In order to identify tidal flare candidates, we begin by compiling a catalog of X-ray point sources and identify the characteristic properties that distinguish such flares from other X-ray point sources such as AGNs, supernovae (SNe), Gamma Ray Bursts (GRBs) and flaring M-dwarf stars. We can expect most variable X-ray sources to be AGNs. Unlike AGNs which typically have a hard power-law spectrum (e.g. Beckmann et al. 2006), tidal flares will have extremely soft ($kT \lesssim 0.1 \text{ keV}$) blackbody spectra. Tidal flares should have much greater variability than AGNs near their peak, but that timescale may be of short ($\lesssim 1 \text{ yr}$) duration. A demonstrated

pre-flare quiescent period as characterized by a lack of significant X-ray emission would also distinguish a tidal flare from an AGN. Redshifted background AGNs, supernovae, GRBs and M-dwarfs may also have soft X-ray emission, but background AGNs may be identified by their optical spectra and M-dwarfs will also produce characteristic optical emission.

X-ray-luminous SNe present a subtle contamination challenge to an archival survey given the likely impracticality of optical follow-up on long timescales and possible lack of sufficient light curve coverage to describe a decay index. But SNe may be eliminated as an explanation through a combination of the flare's peak luminosity and observed rate of decay. SNe and GRBs typically produce X-rays on a timescale of days or months and may be identified optically as well. If the strongest modes of soft, luminous X-ray emission arise first from the prompt shock breakout from the supernova progenitor's surface (e.g. Soderberg et al. 2008), then from the expansion of the ejecta as they interact with the surrounding medium (Schlegel & Petre 2006; Immler et al. 2008), SNe may be correspondingly distinguished from tidal flares.

The most X-ray-luminous SNe due to ejecta expansion (e.g. Immler & Lewin 2003; Schlegel & Petre 2006; Immler et al. 2008) may have long (\gtrsim years) periods of shallow decay. But whether described by thermal or power law spectra, they have not been demonstrated to have peak luminosities significantly in excess of $\sim 10^{42} \text{ erg s}^{-1}$ and typically do not exceed $\sim 10^{40} \text{ erg s}^{-1}$. The progenitor breakout phase may have a supersoft thermal X-ray luminosity in excess of $10^{43} \text{ erg s}^{-1}$, as is also expected from a tidal flare, but this breakout has also shown a fast rise and exponential decay on a timescale of $\sim 100 \text{ sec}$ (Soderberg et al. 2008). Lack of strong variability over timescales of typical *Chandra* or *XMM-Newton* galaxy cluster observations (tens of kiloseconds) should thus exclude breakout from the progenitor as an explanation for a supersoft X-ray flare of comparable luminosity.

The location of the event relative to the host galaxy can be used to rule out a tidal flare event if the location is not consistent with the core of a host galaxy, such as for a supernova outside the galaxy core or a background GRB with no host. As such, we have sought to associate flare candidates with host galaxies using optical data, and to constrain the Rayleigh-Jeans tail of any candidate events with UV data where available.

For our primary dataset, we obtained *Chandra* ACIS archival data for six epochs spanning a period of 8 years, from April, 2000 to March, 2007. In addition, we examined *XMM-Newton* data from December, 2001. X-ray epochs are indicated in Table 1. In order to follow up specific sources, we supplemented our dataset with archival *HST* WFPC2 images with filters F606W and F814W. For our candidate event, we obtained a March 2009 spectrum of the putative host galaxy with the *Hobby – Eberly Telescope* (HET).

2.2. Chandra X-ray Observations

2.2.1. Data Reduction and Candidate Selection

We reprocessed the ACIS event files using *CIAO* to remove pixel randomization. According to standard *CIAO* data processing threads, we also applied TGAIN and CTI

² <http://lisa.nasa.gov/>

corrections, and VFAINT mode cleaning where necessary. We filtered the events to use grades 0, 2, 3, 4 and 6 and energies between 0.3 and 10 keV. During all observations, the target was placed at the ACIS-I aimpoint. All observations used ACIS chips I0-4 and S2, except for obsid 7701 which used the ACIS-I chips only. ACIS suffers from charge readout issues which may be remedied through use of a *destreak* software tool, but the problem is generally only significant on the S4 chip which was inactive in all epochs. We thus did not apply *destreak*. To account for background cosmic-ray induced flares, we filtered individual chips for 3σ deviations using the *CXC* `analyze_ltrcv.sl` script after excluding bright sources found using *wavdetect*. Minor flaring, of duration 20 ksec or longer, was present in all epochs; data from the corresponding time intervals were excluded from further processing.

We defined several bands in accordance with the *ChAMP* definitions found in Kim et al. (2007): B (0.3–8 keV), S (0.3–2.5 keV), H (2.5–8 keV), S1 (0.3–0.9 keV), and S2 (0.9–2.5 keV). In each band, we produced weighted exposure maps and compiled a source list with *wavdetect*. *wavdetect* used a $\sqrt{2}$ scale progression of 1, $\sqrt{2}$, 2, $2\sqrt{2}$, 4, $4\sqrt{2}$, 8 on band images binned by a factor of two, covering a square of width 4096 pixels in physical coordinates that enclosed the whole of the ACIS-I array and hence the cluster core. We used a significance threshold of 10^{-6} for *wavdetect*, corresponding to an approximate maximum of one false source per chip when singly binned, and ~ 1 false source over the whole array when binned by two.

We also created merged, fluxed mosaic images in each band with $1''$ pixels, which we broke into overlapping images with dimensions of 1024×1024 pixels for the purposes of running *wavdetect*.

Once we had compiled a master source list, we eliminated conspicuous edge sources and consolidated redundant multiple detections of single sources across epochs, retaining the astrometric positions that demonstrated the best accuracy. We also eliminated most sources within $0.5' (\sim 95 \text{ kpc})$ of the cluster center, determining them to be unreliable based on *MARX* simulations using a β model for the InterGalactic Medium. We had found these sources to be indistinguishable from Poisson fluctuations in the intracluster diffuse emission. We then visually selected overlapping sources for consolidation, using the 95% encircled energy radii as a guideline and giving preference to positions of detections with larger SNR, or to *Chandra* sources in case of additional detection by *XMM-Newton*.

For initial X-ray source classification, we determined count rates using the Feigelson et al. (2002) polynomial approximations for the 95% encircled energy radius of each epoch, r_{95} and a background annulus between the 99% encircled energy radius r_{99} and $5 \times r_{99}$. We used *dmextract* to determine count rates for each source and determined a subset of sources that across epochs demonstrated (0.3–2.5 keV) variability by a factor of a few, $\gtrsim 4$ –5. All errors use the Gehrels (1986) approximation for Poisson statistics.

Within the set of sources that demonstrated significant variability, we examined basic spectral properties to determine likely soft blackbodies and rule out

AGNs at low-to-moderate redshifts, which we expect to be the most common point source at galactic latitude $b \gtrsim 60$. We define hardness ratios between bands $HR_{1,2} = (c_2 - c_1)/(c_2 + c_1)$ where c_n is the net number of counts in *ChAMP*-defined band n (minimum $c_n = 0$). Given a typical AGN continuum with X-ray photon index $\Gamma \lesssim 2.5$ ($F_X \propto E^{-\Gamma}$), $HR_{H,S2}$ will be sensitive to unusually soft spectra except in the presence of a significant hard background. Even at $L_X(0.3\text{--}8 \text{ keV}) \gg 10^{41} \text{ erg s}^{-1}$, the exponential cutoff on the Wien side of a soft blackbody spectrum will result in few events in the H band, if any. But $HR_{S2,S1}$ will be an exceptional diagnostic for blackbodies in the temperature range anticipated for tidal disruptions if peak emission is somewhere in the vicinity of the *Chandra* bandpass cutoff at $kT \lesssim 0.3 \text{ keV}$.

We also compared variable sources to the Sloan Digital Sky Survey (SDSS) catalog, Data Release 6 (Adelman-McCarthy et al. 2008), eliminating candidates that corresponded to a photometric redshift consistent with background objects ($z \gg 0.2$), most of which were also flagged by SDSS as likely QSOs. We also eliminated stars, determined to be bright non-QSO objects designated as stars by SDSS.

Of the 226 distinct sources we examined, almost all varied in count rate in one or more X-ray bands across epochs, but such variation was usually statistically insignificant. For all but four sources, counting statistics in the hard (2.5–8 keV) band were insufficient to conclusively demonstrate variability. Among the highly variable sources, i.e. those which varied by $\times 4$ or more in B (0.3–8 keV), only a few demonstrated an unambiguous early X-ray *nondetection* (such that the nondetection could not be attributed to the choice of the background extraction region and local background fluctuations), followed by single follow-on rise in photon flux, as well as later flux evolution consistent with steady decline across epochs. Of this subset of sources, only one (source 141) found at $(\alpha, \delta) = 13^h 11^m 22^s, -1^\circ 23' 45''$ (J2000) both demonstrated an unusually soft peak spectrum and was not eliminated via SDSS as a background object, a likely QSO or a foreground star. All other highly variable sources were also associated with AGNs/QSOs or foreground stars, and also had harder spectra ($HR_{H,S} \geq -1.00$). Except for sources 78 and 166, which are associated with SDSS stars that have NOMAD (Zacharias et al. 2005) proper motions $\gtrsim 14 \text{ mas yr}^{-1}$, and source 153 whose variability is inconsistent with a flare’s rise and fall, all other sources have $HR_{H,S} \geq -0.64$.

The X-ray images of the source observed across all epochs and its immediate vicinity are displayed in Figure 1.

For comparison, Table 2 shows a subset containing the 22 most significantly variable sources, such that all had count rates which varied by both at least 2σ and by $\times 4$ over at least 2 epochs of *Chandra* coverage. Due to variations in aimpoint, roll angle and choice of active ACIS chipset across epochs, many sources fell within the *Chandra* FOV for a fraction of the available observations, as indicated in Table 2. Rough broadband (B) count rates and hardness ratios ($HR \equiv HR_{H,S}$) were derived using *dmextract* with a constant extraction radius of $10''$, suf-

ficient to enclose $\gg 90\%$ enclosed energy even at large aimpoint offsets, and a concentric background annulus with twice the area of the extraction radius. Note that for small θ this will introduce additional rate uncertainty, due to the modest size of the background annulus and due to the enclosure of additional background within a larger source extraction radius. But it also improves the tolerance for positional uncertainty which may be an issue for fainter sources.

In Figure 2, we have plotted $HR_{H,S}$ vs. peak count rates from Table 2. Compared against the subset of significantly variable sources not corresponding to stars, source 141 is a clear soft outlier. Most of these non-stellar sources cluster at $HR_{H,S} \sim -0.50$, but source 141 is the lowest.

In very few cases is it possible to place strong limits on the pre-peak absence of an X-ray source. Peak emission in the first epoch of coverage accounts for 8 of these objects. In most cases where the observed peak is later than the first epoch of coverage, manual examination of the event image provides at least some evidence of pre-peak source emission (except for the three objects noted in Table 2). With those sources eliminated from consideration, all remaining significantly variable sources could not have had steady emission stronger than the 1σ detection level of 1.9×10^{-4} ct s $^{-1}$, determined by a single 10 ks observation.

Most objects have one corresponding SDSS object within the *Chandra* PSF (a few $''$). But almost all of these objects have been flagged due to traits that are problematic to interpretation as a tidal disruption. SDSS has flagged 12 optical matches as likely stars due to object morphology and psf modeling, of which 4 are also flagged as potential QSOs due to colors atypical of stars. If these flags are accurate descriptions of the objects in question, they would tend to exclude tidal disruptions in normal galaxies as an explanation for the X-ray variability. Exceptions to this restriction can be imagined, such as if the SDSS observation were near a flare's X-ray peak and captured the blue Rayleigh-Jeans tail in the case of an object flagged as a possible QSO. Bright emission from the center of a relatively faint galaxy might also mimic a stellar radial profile. But without strong evidence from the X-ray emission, the simpler explanation of a star or QSO is preferred. Matches can also be found between 4 of these star-like sources with SDSS correspondences and the 1RXH (ROSAT Scientific Team 2000) and 2RXP (ROSAT Consortium 2000) catalogs, suggesting persistent pre-existing sources rather than new flares.

Excluding all 12 of these flagged objects from Table 2 leaves 10 sources, of which only 3 significantly variable objects are classified as SDSS galaxies. SDSS photometric redshifts indicate source 167 is a likely foreground object, source 157 is a likely background object, and 141 is a plausible cluster member. The 7 other unflagged objects have no corresponding SDSS objects and therefore two possible interpretations. Either they must be background objects which we would not examine as flares for the purpose of this paper (and for which the most likely interpretation is an AGN, given the composition of the X-ray background, see e.g. Giacconi et al. (2001); Szokoly et al. (2004) and references therein), or as dwarf galaxies below the optical detection threshold, for which a tidal flare would remain a possibility of interest. Two

such sources, 134 and 153, appear to have an optical counterpart unregistered by SDSS due to proximity to an image flaw. But for the unmatched sources, the X-ray lightcurves are either too faint or too sparsely sampled to make strong claims as to whether they are the result of tidal disruptions. Including those tagged as possible QSOs, there are 7 star-like SDSS-matched sources which do not have X-ray variability demonstrably inconsistent with a tidal flare. In §4 we will consider those as possible contributors to the flare rate, as well as the 7 unmatched objects, but the available data do not warrant more detailed examination.

The exact behavior of tidal fallback emission remains uncertain and may be expected to harden according to $T_{bb} \propto M_{\bullet}^{-1/4}$ (e.g. Ulmer 1999). But HR indicates an interestingly soft spectrum from the sole likely A1689 cluster member that is both definitely an SDSS galaxy and significantly X-ray variable. According to HR , it is one of the two major soft outliers in the significant variability population (the other of which, source 153, demonstrates erratic light curve behavior clearly inconsistent with the simple rise and fall of a tidal flare).

Having excluded the other X-ray sources from consideration as tidal flare candidates, we will examine source 141 in detail in the remainder of §2 and §3.

2.2.2. Photometry of Source 141

High State:— The source had been observed in obsid 5004 on February 28, 2004. It had been found by *wavdetect* in this *Chandra* epoch only, and there in all bands except H. Within r_{99} , *Chandra* detected a total of 41 counts in the X-ray B band over 19.9 ksec, with an exceptionally soft $HR_{H,S2} = -1.00$ and $HR_{S2,S1} = -0.49$. Within r_{95} this becomes 37 total counts and $HR_{S2,S1} = -0.41$. With an estimated r_{95} background contribution of 5.45 counts, this is a $\sim 9.0\sigma$ detection above background fluctuations with a net rate of $1.6 \pm 0.3 \times 10^{-3}$ s $^{-1}$. Given the H band source emission is indistinguishable from background, this becomes $\sim 11.4\sigma$ when restricted to the S band only.

At $3'.7$ from the cluster core, contributions from the diffuse ICM and faint galactic haloes are sufficiently significant that care must be taken in choosing a background extraction region. Along the radial direction from the cluster core the background varies by a factor of $\gtrsim 2$ within $20''$ of the source for an X-ray B band image of all epochs merged. But the source is sufficiently bright in the 2004 epoch that choosing a background annulus within $5 \times r_{99}$ does not significantly affect source estimates.

Pre-flare:— With no detections of the source in two previous *Chandra* epochs of only 10.5 ksec apiece, we coadded results from obsids 540 and 1663 using epoch-appropriate extractions to determine more stringent upper bounds for a source that is assumed not to be significantly variable. Respectively, the r_{99} count rates are within 0.5σ or less than those of the background extraction annulus. There are no X-ray B band counts within r_{50} for either epoch. Over both pre-flare epochs we find a count rate of 9.5×10^{-5} s $^{-1}$ within r_{95} , still less than the estimated r_{95} background rate of 2.5×10^{-4} s $^{-1}$. We therefore estimate a 1σ upper bound of 1.3×10^{-4} s $^{-1}$ in excess of the background.

Decay:— A much fainter source was also found by *wavdetect* at the same coordinates after the 2004 outburst, but only in the S and S1 bands of obsid 7289 beginning March 9th, 2006. Over 76 ksec there are 51 total and 11.33 net X-ray B band counts within r_{99} . Using smaller extraction radii results in the loss of a small fraction of the source counts but also reduces contributions due to background, which generally increases with increasing radii due to an increased fraction of the brighter core regions of the ICM. Thus, in determining the significance of the March 2006 emission, which is faint with respect to the background, we use the 90% encircled energy radius enclosed by a background annulus out to $2 \times r_{90}$. From the March 9th, 2006 observations, we find 28 total and 11.48 net X-ray B band counts within 76 ks, i.e., $\sim 2.2\sigma$ above background. Although there is no detection from obsid 6930 on March 6th, 2006, we similarly find 18 total and 6.98 net counts within 77 ks, i.e., $\sim 1.7\sigma$ above background. The two March 2006 observations are separated by a time interval equivalent to their combined duration, i.e., much smaller than the ~ 2 yr elapsed from obsid 5004. Because of this short separation, we henceforth treat obsids 6930 and 7289 as a single 153 ks observation, which leads to a $\sim 3\sigma$ detection of the source with a count rate of $1.2 \pm 0.5 \times 10^{-4} \text{ s}^{-1}$.

At only 5 ksec, obsid 7701 produced no detection of the source and no photons within r_{95} on March 7, 2007. Taking the emission to be background, we estimate the 1σ upper bound of $3.7 \times 10^{-4} \text{ s}^{-1}$ in excess of the background.

Variability:— In order to confirm the degree of variability, we used the *CIAO* tool *glvary*, which characterizes a Bayesian analysis of Poisson statistics with a variability index (VI) based on an $\log_{10}(O)$ where O is the odds ratio (Gregory & Loredo 1992; Rots 2006). Examining both the X-ray S and B bands across all epochs and across expected rise and fall times, we find $VI \geq 8$ and $O > 5.9$ in all cases, where $VI \geq 6$ is considered definitely variable and the maximum VI is 10. The source shows no significant variability within its high-state epoch, obsid 5004.

2.2.3. Least Squares Spectral Fitting

We fitted the spectra from the high and post-decay states (from February 2004 and March 2006, respectively) using *XSPEC* v12.4.0 (Arnaud 1996; Dorman & Arnaud 2001) with a variety of blackbody and power law models that include absorption by line-of-sight neutral hydrogen³ and Churazov et al. (1996) weighting. We assumed that the source was a member of the cluster at fixed $z \sim 0.183$, although z did not change by more than a few percent when left free to vary. For spectral fitting we used 99% encircled energy extraction radii and account for *Chandra* ACIS instrumental response by calculating position-dependent response matrices using *mkrmf* and *mkarf*.

We found the high state emission fitted well a blackbody of temperature of $kT_{bb} = 0.12 \pm 0.02 \text{ keV}$, with

³ Due to the relatively low redshift of the object, it does not matter if the absorption is assumed to be in our galaxy or the external galaxy. For simplicity we assume the absorption all takes place within our galaxy for the purposes of spectral fitting.

$\chi^2/\nu = 5.89/5.00$. Fixing kT_{bb} at this value, we estimate an X-ray flux. $F_X(0.3\text{--}10 \text{ keV}) = 3.7 \pm 1.4 \times 10^{-14} \text{ erg cm}^{-2} \text{ s}^{-1}$, with negligible contribution above 2 keV. Fitting tended to decrease estimated N_H below the galactic values found by Dickey & Lockman (1990) to unphysically low numbers, so we froze N_H at the *colden* value of $1.82 \times 10^{20} \text{ cm}^{-2}$. Corrected for galactic extinction, $F_X(0.3\text{--}10 \text{ keV}) = 4.7 \pm 1.7 \times 10^{-14} \text{ erg cm}^{-2} \text{ s}^{-1}$.

The fit for a power law produced a photon index $\Gamma = 4.86 \pm 0.48$ with a modestly better fit, $\chi^2/\nu = 5.36/5.00$ and uncorrected $F_X(0.3\text{--}10 \text{ keV}) = 5.6 \pm 2.5 \times 10^{-14} \text{ erg cm}^{-2} \text{ s}^{-1}$, 99.5% of which is below 2 keV. Allowing N_H to vary freely increases it to $1.07 \pm 0.41 \times 10^{21} \text{ cm}^{-2}$ with $\Gamma = 5.8 \pm 3.5$, $\chi^2/\nu = 4.98/5.00$ and uncorrected $F_X(0.3\text{--}10 \text{ keV}) = 5.6 \pm 2.5 \times 10^{-14} \text{ erg cm}^{-2} \text{ s}^{-1}$.

For the decayed state, blackbody fitting produces 1σ upper limits of $N_H = 1.6 \times 10^{22} \text{ cm}^{-2}$ and $kT_{bb} = 0.17 \text{ keV}$ with $\chi^2/\nu = 8.35/9.00$, consistent with high state properties, and a model $kT_{bb} = 0.10 \pm 0.02$, if we fix N_H during the fit at the observed galactic value. If we assume no change in spectral shape over 2 years, we estimate an uncorrected $F_X(0.3\text{--}10 \text{ keV}) = 4.1 \pm 2.8 \times 10^{-15} \text{ erg cm}^{-2} \text{ s}^{-1}$. Corrected for galactic extinction, $F_X(0.3\text{--}10 \text{ keV}) = 5.1 \pm 3.5 \times 10^{-15} \text{ erg cm}^{-2} \text{ s}^{-1}$.

A power law fit for the post-decay state with galactic N_H gives $\Gamma = 5.7 \pm 1.1$, $\chi^2/\nu = 8.93/10.00$ and uncorrected $F_X(0.3\text{--}10 \text{ keV}) \lesssim 1.4 \times 10^{-14} \text{ erg cm}^{-2} \text{ s}^{-1}$. Γ cannot be reasonably constrained, if N_H is left free to vary.

An overlaid spectrum of a simultaneous blackbody fit of the high and low states is presented in Figure 3. If we assume the combined source flux from pre-flare epochs represents an approximately constant background, we can fit it to high state blackbody temperature, N_H and redshift. This fit predicts no pre-flare source $F_X(0.3\text{--}10 \text{ keV})$ with a 1σ upper bound $6.9 \times 10^{-15} \text{ erg cm}^{-2} \text{ s}^{-1}$. Corrected for galactic extinction, $F_X(0.3\text{--}10 \text{ keV}) \leq 8.6 \times 10^{-15} \text{ erg cm}^{-2} \text{ s}^{-1}$. If we use r_{90} to reduce likely background contamination of this estimate, we find an extinction-corrected limit of $1.6 \times 10^{-15} \text{ erg cm}^{-2} \text{ s}^{-1}$. With a much shorter observation time than any epoch, we can constrain the post-flare flux from the March 2007 epoch only very roughly. Using similar methods to those by which we estimate the pre-flare flux, even 0 counts within r_{95} lead to a blackbody extinction-corrected $F_X(0.3\text{--}10 \text{ keV}) = 8.3 \times 10^{-15} \text{ erg cm}^{-2} \text{ s}^{-1}$ or a 1σ upper bound of $3.5 \times 10^{-14} \text{ erg cm}^{-2} \text{ s}^{-1}$ for 4 counts within r_{99} in a single energy bin.

2.3. Supplementary Observations

2.3.1. XMM-Newton Data

Pipeline processing for *XMM-Newton* found no corresponding X-ray source for the 40 ksec December 2001 epoch. Our examination of the MOS and PN event files and the composite broadband image (0.2–12.0 keV) found no evidence of a source within *XMM-Newton* r_{80} , which at $\sim 20''$ is significantly larger than the *Chandra* positional uncertainty. The mean value of the pipeline sensitivity map within r_{80} is 0.0022 s^{-1} , equal to the 3σ upper limit of the encircled photons. We fitted a PN spectrum generated using the *espec* tool from the *XMM-Newton* SAS software suite, version 7.1.0. For a 1σ black-

body with peak kT_{bb} , N_H and redshift, we find an uncorrected upper limit $F_X(0.3\text{--}10\text{ keV}) = 8.5 \times 10^{-16} \text{ erg cm}^{-2} \text{ s}^{-1}$ or extinction-corrected $F_X(0.3\text{--}10\text{ keV}) = 1.1 \times 10^{-15} \text{ erg cm}^{-2} \text{ s}^{-1}$. This source region is also included with the *Chandra* data in Figure 1.

We also examined optical and ultraviolet images observed using the *XMM-Newton* Optical Monitor with the filters UVW2 (1800Å–2300Å), UVW1 (2300Å–3700Å), U (3000Å–3900Å), and B (3800Å–4900Å). The region within $\sim 2'$ of the source is dominated by a ghost ring in the Optical Monitor, an artifact of increased background due to reflection of stray light from a bright source. This contamination dominates across all filters and prevents extraction of useful optical or ultraviolet data.

2.3.2. SDSS and CTIO Data

We examined the Sloan Digital Sky Survey Catalog from Data Release 6 (Adelman-McCarthy et al. 2008) to eliminate flaring red dwarfs as a possible explanation for variable, extremely soft emission within our field and found several such objects corresponding to otherwise interesting X-ray candidate sources. From our softest sources we found one SDSS object designated a galaxy by PSF modeling that corresponded to the *Chandra* *wavdetect* position of SDSS J131122.15-012345.6. This galaxy was observed on March 3, 2000 and found to have SDSS *ugriz* magnitudes of $u = 25.27 \pm 1.14$, $g = 21.45 \pm 0.07$, $r = 20.46 \pm 0.04$, $i = 20.10 \pm 0.05$, $z = 19.63 \pm 0.11$. The large u error is likely due to being a nondetection in the u -band, which we confirmed by examination of *ugriz* band images. Note that the characteristic limiting magnitude for SDSS in the u -band is 22.3 so the uncertainty is likely even higher.

SDSS Photometric redshifts vary by ~ 0.23 depending upon the method used but suggest the galaxy is likely a member of A1689 given the much smaller odds of a foreground nonmember and typical unreliability of blind photometric redshifts at $z \ll 1$. The SDSS template fitting algorithm finds a redshift of $z = 0.097 \pm 0.03$ whereas the catalog's neural network derived redshifts are $z = 0.20 \pm 0.09$ and $z = 0.33 \pm 0.07$ for the CC2 and ZD1 methods respectively. We have also run our own photometric redshift estimates, finding $z = 0.16 \pm 0.09$ using ANNz neural networking software (Collister & Lahav 2004).

We estimated the redshift with LePhare template fitting software (Ilbert et al. 2006) and its Hubble Deep Field North libraries. By incorporating CTIO J- and K-band data from Stanford et al. (2002), where $M_J = 19.12 \pm 0.12$ and $M_K = 17.02 \pm 0.11$, we find an effective upper bound of $z = 0.20$ and a most likely model of an elliptical galaxy. The redshift probability distribution is bifurcated with maxima at $z = 0.04$ and 0.20 . The upper maximum reflects an Sa model, which fits $z = 0.19 \pm 0.04$ if the elliptical model is eliminated from consideration, and a bolometric absolute magnitude $M_{bol} = -20.17$ at that redshift. Redshift $z = 0.04$, on the other hand, would imply $M_{bol} = -16.29$. The fit cannot exclude the possibility of a QSO at $z \simeq 3.44$ which assumes Ly α emission that is undetected in the gap between the g and r bands.

2.3.3. HST-WFPC2

We retrieved archival images from the Hubble Space Telescope taken using the Wide Field Planetary Camera. SDSS J131122.15-012345.6 was observed as part of Abell 1689 by WFPC2 for multiple ≥ 900 s orbits on March 2, 1996 and July 4, 1996 using the F606W and F814W filters, although a single orbit from each filter was sufficient for our purposes. To improve relative astrometry, we shifted the HST image to align with *Chandra* coordinates. We determined the centroid coordinates of other bright X-ray sources within the WFPC2 FOV and visually identified the centers of corresponding HST objects that also had SDSS catalog entries. SDSS objects corresponded reliably to *Chandra* objects and were much more numerous than *Chandra* objects, so we used additional SDSS objects to confirm HST correspondence. We find the centroid of the *Chandra* source to be within a *Chandra* pixel ($0''.5$) of the host object's center, but the primary source of positional error is the statistical uncertainty in the centroid of the X-ray source, $\sim 1''.8$. The correspondence of the galaxy to the *Chandra* X-ray source can be seen in Figure 4. Later we will assume the X-ray source is indeed associated with SDSS J131122.15-012345.6 unless explicitly stated otherwise.

We confirmed the host object as a galaxy whose morphology appears plausibly elliptical but exhibits some spiral symmetry, possibly containing spiral arms that are either broad or too smooth to definitively demarcate at the galaxy distance. Using IDL user-contributed programs (Landsman 1993; Barth 2001) for aperture photometry and fitting the flux to a Sérsic (1963) $R^{1/n}$ radial profile, we found a Sérsic index $n \simeq 1.2$, which suggests dominance by an exponential disk model (see, e.g. Blanton et al. (2003); Graham & Driver (2005)). The flux in excess of an $n = 1$ profile lies within $\sim 0''.15$ of the center (a 3×3 grid of detector pixels) and suggests a maximum bulge-to-total luminosity ratio B/T = 0.18. The radial profile is a poor fit to a deVaucouleurs profile where $n = 4$, even excluding the core excess, suggesting the galaxy is not elliptical. We further confirm a spiral disk-and-bulge model by examining the ratio of F606W to F814W as a function of radius. The ratio is approximately flat as a function of radius except within the region of core excess, where it demonstrates a sudden red spike as might be produced by a spiral galaxy with a red core and as opposed to a more gradual reddening in an elliptical. We conclude, therefore, the galaxy is most likely a spiral.

2.3.4. HET

We observed SDSS J131122.15-012345.6 using the *Hobby-Eberly Telescope* (HET) for a total of 5900 seconds split into 4 sub-exposures. The first two were taken on March 24, 2009 and the other two on March 27, 2009, well after we would expect to see any emission lines due to the tidal flare itself. We used the LRS (low-resolution spectrograph) with the G1 grism (300 l/mm) and the $2''$ slit. This gave us a resolution of 14.8Å or 800 km/s at 6000 Å . The spectrum covered the range $4080 - 10800 \text{ Å}$, with the peak sensitivity between 5500 and 6000 Å . The signal-to-noise ratio (hereafter S/N) in this spectrum is approximately 4 at 5000 Å , 7 at 5300 Å , approximately flat at a value of 10 between 5500 and 7200 Å , and drops to values of 3–6 between 7500 and 8500 Å . At the longest

wavelengths, the noise is dominated by imperfect subtraction of the strong OH emission lines in the spectrum of the sky background.

Absolute spectrophotometry with the HET can suffer from large errors because a variable fraction of the light incident on the primary mirror is focused onto the secondary as it tracks the object across the field of view. Therefore, we have adjusted the absolute flux scale by in order to match the SDSS photometry. After diving the original flux scale by 2.75 we achieve a very good agreement with the r , i , and z magnitudes. The observed spectrum is shown in Figure 5. By comparison with the spectrum of the nearby elliptical galaxy NGC 3379, We identify features that we interpret to be the Na I D interstellar double near 7000Å and the Ca II H and K lines near 4650Å at target-redshifted wavelengths, as well as Mg I b absorption near 6170Å. Thus, we find $z = 0.195$, in good agreement with photometric results from *LePhare*. These features are marked and labeled in Figure 5. The signal-to-noise ratio is insufficient to eliminate ambiguity from the redshift estimate, in part due to the lack of strong emission lines. This redshift is supported by template fitting with the *EZ* tool that was used in the VIMOS VLT Deep Survey (VVDS, Le Fèvre et al. 2005) and includes spectral line identification capabilities. The best fits are for elliptical templates which also confirm absorption in Ca II and Mg I b, as well as the G band, H γ and H β near 5139Å, 5186Å and 5809Å. A starburst model also reproduces this redshift but with a continuum significantly bluer than observed. None of the *EZ* AGN models converged at the redshift of the object (V. Le Brun 2009, private communication).

In order to evaluate the possibility that emission lines form an AGN are hiding in the optical spectrum, we have determined upper limits on the flux of some of the relevant lines. In particular, we have focused on the observed wavelength range 5800–6000 Å, where we expect to find the H β and [O III] $\lambda\lambda 4959, 5007$ emission lines (marked and labeled in Figure 5). This also happens to be the region of the spectrum where the S/N is highest. Although the H α line is stronger than H β , it falls at an observed wavelength of 7843 Å, where the noise is very high. The positive spikes discernible in this part of the spectrum are a result of poor subtraction of emission lines from the night sky. We expect the [O III] lines to be unresolved, therefore, we assume a FWHM of 800 km s⁻¹ according to the spectral resolution attained in the spectrum. Under this assumption we obtain an upper limit to the observed flux of the [O III] $\lambda 5007$ line of 1×10^{-16} erg s⁻¹ cm⁻². If a line is stronger than this limit, its peak stands out by more than 3σ above the local noise. In the case of the H β line, we considered two different values of the FWHM, 900 km s⁻¹ (marginally resolved) and 1600 km s⁻¹. We chose these particular values because they are typical of the H β lines of Narrow-Line Seyfert 1 galaxies (hereafter NLS1s), which are known for their large-amplitude X-ray variability (e.g. Boller et al. 1993, 1997; Grupe et al. 1995a, 2008a). Thus the limits we obtain under these assumptions will be relevant to our discussion of whether the observed flare could be an example of dramatic variability in a NLS1 galaxy. For a FWHM of 900 km s⁻¹ the upper limit to the H β is 1×10^{-16} erg s⁻¹ cm⁻² (just as for the

[O III] $\lambda 5007$ line), while for a FWHM of 1600 km s⁻¹ the upper limit to the H β is 2×10^{-16} erg s⁻¹ cm⁻². For line broader than this, the upper limit to the integrated flux increases proportionally to the FWHM.

2.3.5. GALEX

Ultraviolet observations of SDSS J131122.15-012345.6 using the *Galaxy Evolution Explorer*⁴ (*GALEX*) exist for the dates of 22 April 2004 and 24 April 2007. These ~ 100 s survey observations have limiting magnitudes of $\sim 20 - 22$ for bands about ~ 1500 Å and ~ 2300 Å. No emission is obviously visible by inspection at the location of the galaxy in either band, whether from the galaxy as a whole or a point within the galaxy. But given the limiting magnitude of these short observations, they should be insufficient to detect even an unabsorbed 0.12 keV blackbody emitting $\lesssim 4.7 \times 10^{-14}$ erg cm⁻² s⁻¹, as derived from the *Chandra* spectrum of 28 February 2004. Furthermore, the galaxy lies at $\sim 3'$ of either field's edge and is thus flagged for instrumental issues due to rim proximity.

3. DISCUSSION

3.1. Observational and Theoretical Background

In order to place our new results in context, we first provide brief reviews of both previous observations and estimates of tidal flare rates.

Although we expect tidal disruption flares to be among the most luminous observable astrophysical events, with the total kinetic energy of ejected debris exceeding that of supernovae at 10^{51} erg or more, these flares have thus far been challenging to observe. While they should occur within AGNs and may contribute significantly to the faint end of the AGN X-ray luminosity function (Milosavljević et al. 2006), they will be easiest to identify in a quiescent galaxy, where they can be distinguished from typical variable disk accretion in an AGN.

Existing theoretical studies predict disruption rates of 1 event per $10^4 - 10^5$ years per galaxy, (e.g. Magorrian & Tremaine 1999), a rate that has been supported by observational studies using ROSAT (Donley et al. 2002). The most optimistic predictions increase that rate by an order of magnitude (Wang & Merritt 2004).

Several candidate events have been observed (Komossa 2005; Komossa et al. 2004; Halpern et al. 2004), but some of the most convincing evidence of tidal disruptions comes from *GALEX* detections of UV flares with optical and X-ray component as observed by Gezari et al. (2006, 2008b, 2009). Ongoing studies using the XMM Slew Survey (Esquej et al. 2007, 2008) also report candidate events, but an extensive study of the Chandra Deep Field (Luo et al. 2008) made no detections, consistent with maximum rates comparable to 10^{-4} per galaxy per year for $L \gtrsim 10^{43}$ erg s⁻¹. Since only about a dozen such candidate events have been identified to date (see the above references), the statistical conclusions that can be reached thus far are highly tentative.

The rate by which tidal flares occur should also act as an indicator for the distribution of black holes in the galaxy population. The effect may be particularly

⁴ <http://www.galex.caltech.edu>

pronounced according to the theoretical calculations of Wang & Merritt (2004) if a significant fraction of nucleated dwarf spheroidal galaxies harbor MBHs at their centers. Given that dwarf ellipticals are a very numerous component of the galaxy distribution (see, for example Jenkins et al. 2007), if lower mass MBHs flare more often than more massive MBHs, they may dominate the flare rate if they contribute at all. But more recent work by Merritt (2009) suggests lower mass MBHs may produce such flares more rarely even if dwarf galaxies do possess MBHs. As noted in the introduction, determining the population of MBHs in dwarf spheroids through such indicators as tidal disruption events will also affect predicted rates of MBH-MBH mergers and extreme mass ratio inspirals (EMRIs). Although the gravitational wave detector *LISA* will be sensitive only to disruptions of stars with compact cores (Amaro-Seoane et al. 2007), as indicators of the dwarf galaxy MBH population these predicted rates will have additional implications for *LISA*, which will be sensitive to deeply penetrating encounters in the mass range of $M_{\bullet} \lesssim 10^7 M_{\odot}$ (Jennrich 2004; Sesana et al. 2004, 2005; Sigurdsson 2003).

3.2. Derived Galaxy Properties

3.2.1. Cluster Membership

With a spectroscopic estimate of $z = 0.195$ for SDSS J131122.15-012345.6, we take the galaxy to be a member of Abell 1689. A variety of redshift estimates have been published for Abell 1689 ranging from 0.183 (Struble & Rood 1999) to 0.203 (Estrada et al. 2007). The high velocity dispersion of this massive cluster suggests that membership of the SDSS galaxy is plausible even for a low estimate of the cluster redshift. Halkola et al. (2006), for example, estimate a velocity dispersion $\sigma \sim 1500 \text{ km s}^{-1}$, placing the galaxy in the upper $\sim 1\%$ of cluster members for the low z estimate. Duc et al. (2002) define an inclusive cluster range of $z = 0.17 - 0.22$ using both photometric and spectroscopic redshifts. And Martini et al. (2007) estimate $\sigma = 2402 \text{ km s}^{-1}$ for $z = 0.1867$. For the purpose of calculating luminosities then we select a characteristic redshift $z = 0.19$ for which the luminosity error will be a factor of less than 1.09 whether or not the SDSS galaxy's higher measured redshift signifies Hubble expansion rather than motion relative to the cluster center. In our adopted cosmology, $z = 0.19$ corresponds to a luminosity distance of 926 Mpc.

3.2.2. Black Hole Mass

Since we do not have a measurement of the stellar velocity dispersion of the host galaxy, we have used photometry to estimate the mass of its central black hole (assuming it has one). We estimated M_{\bullet} from M_V as per Lauer et al. (2007), as well as from M_B as per Ferrarese & Ford (2005). We determine M_V and M_B from SDSS *ugriz* magnitudes and the conversion method prescribed by Lupton (2005). We specifically use the calculations that rely upon the *g* and *r* bands only given the likely unreliability of *u*. We have not applied K-corrections as the adjustments they introduce at $z = 0.19$ will be minor compared to the errors resulting from scatter in the photometric $M_{\bullet} - L$ relation. Using the ratio of bulge luminosity to total galaxy luminosity

(B/T) based on the SDSS data, we find for the bulge $M_V = -17.10 \pm 0.10$ and $M_B = -15.98 \pm 0.10$.

We then refer to Lauer et al. (2007) and Ferrarese & Ford (2005) to estimate M_{\bullet} . Given $M_V = -17.10$, we use the Lauer et al. (2007) relation that includes their entire dataset, and is hence appropriate for $M_V > -19$. This relation implies $\log(M_{\bullet}/M_{\odot}) = 6.23 \pm 0.29$, and the Ferrarese & Ford (2005) relation produces $\log(M_{\bullet}/M_{\odot}) = 6.68 \pm 0.24$. Taking the mean from these relations we find $\log(M_{\bullet}/M_{\odot}) = 6.46 \pm 0.38$, an estimate that is comfortably compatible with the possibility of tidal disruption events, even if a much larger error were inferred due to the inherent uncertainty in estimating (B/T). The indicated error arises primarily from scatter in the relations we reference, but our ability to measure (B/T) is limited by WFPC2 pixel scale. For example, the host galaxy could have a more compact bulge and hence a lower inferred black hole mass. We therefore determine the largest uncertainty in the lower bound of M_{\bullet} by assuming that the bulge is described by a single pixel. In this case, the additional uncertainty due to (B/T) is $\Delta \log(M_{\bullet}/M_{\odot}) \propto \log(B/T) \sim 0.4$.

3.3. Was the Event a Tidal Flare?

In the following subsections we argue that alternative explanations of the observations are disfavored by the data. We then demonstrate that the data are consistent with the event being a tidal flare.

3.3.1. A Galactic Foreground Object?

At a galactic latitude of 61° , the position of Abell 1689 already produces a relatively low probability of having a line-of-sight foreground object e.g. a distant M-star. We now consider the following: (1) A source within the galactic plane, at a distance of $\sim 1 \text{ kpc}$, would have $L_X(0.5-2.5 \text{ keV}) \lesssim 10^{30} \text{ erg s}^{-1}$, whereas known quiescent low-mass X-ray binaries (qLMXBs) typically have $L_X(0.5-2.5 \text{ keV}) > 10^{31} \text{ erg s}^{-1}$ and hard spectra, $\Gamma \sim 1 - 2$ (Heinke et al. 2003). (2) M-dwarfs are considerably more common and occasionally produce X-ray flares, but even a faint galactic M-dwarf should be visible against our proposed host galaxy for the event in HST image (take, for example, the M-dwarf selection criteria of $r < 19.0$ by SEGUE, (Yanny et al. 2009)).

3.3.2. A Highly Variable AGN?

We consider alternate extragalactic explanations for the X-ray flare due to known types of X-ray emitting objects. For example, AGNs may show X-ray variability of a factor of a few but typically not bright outbursts of $\gtrsim 30$. Characterization of the X-ray continuum and the observed power law of $\Gamma \gtrsim 5$ is also atypical of AGNs, which are better described by $\Gamma \lesssim 2.5$ (e.g. Beckmann et al. 2006), save for NLS1s. Although photometric fitting is consistent with a QSO at $z \sim 3.4$, luminous AGNs typically have prominent emission lines at optical rest wavelengths whereas the host shows no strong emission lines in the HET spectrum with limits as reported in §2.3.4. A template fit requiring a photometric redshift $z \sim 3.4$ is also contraindicated by the HET redshift, $z = 0.195$. Given the optical spectral information, we judge therefore that an AGN is unlikely to

have caused of the observed flare, with the following two exceptions: BL Lac objects and Narrow-Line Seyfert 1 galaxies (NLS1s, known for their steep soft X-ray spectra and rapid X-ray variability). We consider these two possibilities in turn.

A BL Lac Object. – There exists no corresponding radio source in the FIRST catalog (White et al. 1997) as would be expected for a BL Lac. (For a review of BL Lac properties, see Urry & Padovani 1995). The FIRST catalog reaches a sensitivity 0.75 mJy at 1.4 GHz and includes the *Chandra* fields. Given that most BL Lac objects have elliptical galaxies as hosts, the favored spiral classification of the host galaxy also implies the flare does not arise from a BL Lac object.

A Narrow-Line Seyfert 1 Galaxy or Similar Object? – There are a number of examples of NLS1 galaxies displaying dramatic X-ray variability (with amplitudes of more than a factor of 10). These include WPVS 007, which showed a drop in its soft X-ray flux by a factor of ~ 400 in 3 years (Grupe et al. 1995a), and Mrk 335, which showed a drop in its soft X-ray flux by a factor of ~ 30 in approximately 1.4 years (Grupe et al. 2008a). X-ray variability by a factor of up to 10 on time scales as short as days is a trademark of NLS1s (see, for example, the light curves of NGC 4051 in McHardy et al. 2004). An extreme example of this type of behavior is the variability of IRAS 13224–3809 (Boller et al. 1993, 1997). There are also examples of dramatic X-ray flares in AGNs that are not NLS1s, including IC 3599 (also known as RE J1237+264 or Zwicky 159.034) and NGC 5905. Both of these are Seyfert 2 galaxies with X-ray excursions by factors of 120 and 150 respectively (see Grupe et al. 1995b; Brandt et al. 1995; Bade et al. 1996; Komossa & Bade 1999; Gezari et al. 2003).

The characteristic broadband spectral properties of SDSS J131122.15-012345 are generally not unheard of among NLS1s, but they are atypical in several respects. Like NLS1s in general, its X-ray emission is very soft. The vast majority of NLS1 X-ray spectra, however, can be fit with power laws such that $\Gamma \sim 2-4$ (Grupe 2004). Both high and low states of SDSS J131122.15-012345.6 are fit to power laws with $\Gamma \sim 5$, which is comparable to the softest examples from Brandt et al. (1995) and moderately steeper than these examples of dramatic Seyfert flares, with the dramatic exception of WPVS 007 ($\Gamma \sim 10$) which has been attributed to the presence of a warm absorber (Grupe et al. 2008b). The correlation between spectral slope and L_X observed by Grupe (2004) is more problematic for classifying SDSS J131122.15-012345 as an NLS1. The softest object in that sample corresponds to $L_X \sim 10^{44}$ erg s $^{-1}$, $\sim 4\times$ brighter than the observed high state power-law $L_X(0.2-2.0$ keV) of SDSS J131122.15-012345. This high state $L_X(0.2-2.0$ keV) conversely corresponds to $\Gamma \sim 2.5$ in the Grupe (2004) sample, compared to the observed $\Gamma \sim 5$. The low state Γ is similarly steep, consistent with no time evolution, and more difficult to reconcile with this $\Gamma - L_X$ relationship. Examining the properties of the optical continuum, we find that the SDSS *g*-band absolute magnitude $M_g = -18.4$ is low for the sample examined by Zhou et al. (2006), who find that soft optically selected NLS1s almost exclusively occupy $-19 \lesssim M_V \lesssim -25$. This M_g corresponds to a HET spectrum that declines

steadily with decreasing λ for $\lesssim 5500\text{\AA}$ (SDSS color $(u-g) \sim 3.8$), which would make a similar NLS1 rare and "UV-deficient" compared to a typical flat-spectrum NLS1 in (Zhou et al. 2006).

To investigate whether the observed flare in SDSS J131122.15-012345.6 is consistent with the variability of an AGN, we ask whether optical emission lines characteristic of an AGN could be hidden in its optical spectrum below our detection limit. To answer this question, we have studied the relation between the 0.2–2.0 keV X-ray luminosity and the (broad) H β and (narrow) [O III] $\lambda 5007$ line luminosities among the 51 NLS1 galaxies in the sample of Grupe et al. (2004). In this sample, the ratio $F_X(0.2-2\text{ keV})/F(\text{H}\beta)$ has a median value of 127, with 90% of objects having $F_X(0.2-2\text{ keV})/F(\text{H}\beta) > 50$. Similarly, the ratio $F_X(0.2-2\text{ keV})/F([\text{O III}])$ has a median value of 486, with 90% of the objects having $F_X(0.2-2\text{ keV})/F([\text{O III}]) > 100$. Using the best-fitting power-law model for the spectrum of SDSS J131122.15-012345.6, we find that in the quiescence $F_X(0.2-2\text{ keV}) < 5.1 \times 10^{-15}$ erg cm $^{-2}$ s $^{-1}$, implying that $F(\text{H}\beta) < 1 \times 10^{-16}$ erg cm $^{-2}$ s $^{-1}$ and $F([\text{O III}]) < 5 \times 10^{-17}$ erg cm $^{-2}$ s $^{-1}$ (at 90% confidence), which fall just below our detection limit. However, we doubt that this object can be a NLS1 galaxy because the upper limit on its quiescent X-ray luminosity suggests that any AGN should be accreting at a rate well below the Eddington limit, contrary to NLS1s. In particular, using the Elvis et al. (1994) spectral energy distribution as a template, the upper limit on the quiescent X-ray luminosity, and the black hole mass derived above, we infer an upper limit on the Eddington ratio in quiescence of $L_{\text{bol}}/L_{\text{Edd}} < 0.01$. In contrast NLS1 galaxies have $L_{\text{bol}}/L_{\text{Edd}} > 0.1$ (e.g. Mathur & Grupe 2005). Considering now the cases of the Seyfert 2 galaxies, IC 3599 and NGC 5905, we notice that *in their high X-ray flux states* they had $F_X(0.2-2\text{ keV})/F([\text{O III}]) = 240$ and 10 respectively. If these values are representative and if SDSS J131122.15-012345.6 is a similar object, we would expect it to have $F([\text{O III}]) \approx (1-30) \times 10^{-15}$ erg cm $^{-2}$ s $^{-1}$ (since it has $F_X(0.2-2\text{ keV}) = 2.7 \times 10^{-13}$ erg cm $^{-2}$ s $^{-1}$ for a power law in its high state). These line fluxes are an order of magnitude above our detection limit, yet we have not detected any lines, which leads us to conclude that SDSS J131122.15-012345.6 is unlike IC 3599 and NGC 5905. Rather it resembles RX J1242.6-1119 (Komossa & Greiner 1999) and RX J1624.9+7554 (Grupe et al. 1999), which are apparently normal galaxies that exhibited large, soft X-ray flares with amplitudes of 20 and 235, respectively. Of course, without additional observational constraints near the flare peak we cannot entirely exclude the possibility that, despite having excluded known modes of AGN emission and variability, we have found an extremely rare instance of supersoft variability from a quiescent or obscured AGN and not a stellar tidal disruption. Explanations might include a novel mode of fluctuation in an otherwise low-luminosity (perhaps radiatively inefficient) accretion flow or a temporary gap in obscuring material.

3.3.3. Other Extragalactic Line-of-Sight Objects?

As described in §2.1, supernovae have been observed rarely to emit prompt X-ray flashes that reach luminosities comparable to those observed in the candidate flare, such as from a progenitor shock breakout (Campana et al. 2006; Soderberg et al. 2008; Gezari et al. 2008a). In all cases, the soft thermal component that dominates this prompt flash evolves rapidly over timescales of less than the 20 ks peak observation of our candidate flare. This evolution appears to occur in conjunction with a softening of kT_{bb} as the breakout expands into larger distances from the progenitor surface. The A1689 flare demonstrates no such short-term variability during the peak epoch, excluding a progenitor breakout as an explanation. The flare is also orders of magnitude more luminous than even more luminous examples of later, long-term evolution of supernova ejecta (Immler & Lewin 2003; Schlegel & Petre 2006; Immler et al. 2008), suggesting that a different explanation is also necessary here.

X-ray afterglows from gamma ray bursts (GRBs) have been observed on time scales of years (Grupe et al. 2010) but the decay is sufficiently rapid (declining a factor of 10^5 within 10^5 s of peak X-ray luminosity, then another factor of 10^5 by 10^8 s) and the X-ray spectrum sufficiently hard ($\Gamma \sim 1$) that we reject them as explanations for the event we detected.

3.3.4. Tidal Flare Explanation

We now compare our result to previously reported events. Early *Chandra* observations of SDSS J131122.15-012345.6 indicate no detectable source for observations of at epochs 2000.29 and 2001.98 with $L_X(0.3-3 \text{ keV}) < 1.6 \times 10^{41} \text{ erg s}^{-1}$ at $z = 0.19$. The *XMM-Newton* observation places a similar limit of $1.1 \times 10^{41} \text{ erg s}^{-1}$ at epoch 2001.98. Then, we detected a prominent $\sim 11\sigma$ super-soft flare with an extinction-corrected $L_X(0.3-3 \text{ keV}) = 4.8 \times 10^{42} \text{ erg s}^{-1}$ at $t = 2004.16$, as well as evidence ($\sim 3\sigma$) of emission two years later at $t = 2006.18$ with $L_X(0.3-3 \text{ keV}) = 5.2 \times 10^{41} \text{ erg s}^{-1}$. At $t = 2007.18$, $L_X(0.3-3 \text{ keV}) < 3.6 \times 10^{42} \text{ erg s}^{-1}$. Unless otherwise indicated, further values of L_X for this flare will use a value as determined from a 0.12 keV blackbody in the 0.3–3 keV band, corrected for extinction through the plane of our galaxy as per §2.2.3.

The peak observed X-ray luminosity and temperature are as predicted by theory and typical for X-ray observations of tidal flare candidates to date (see Gezari et al. (2009) for a review and refer to their Figure 10), and the rise in luminosity by a factor of ~ 30 over pre-flare background is typical but not remarkable. For example, Esquej et al. (2008) consider candidates with $L_X(0.2-2 \text{ keV})$ variable by $\times 20$ and Luo et al. (2008) require a count rate variable by > 20 , but we see a factor of $\gtrsim 650$ in $L_X(0.3-2.4 \text{ keV})$ for Cappelluti et al. (2009).

The observed L_X never approaches theoretical peak luminosities of $> 10^{45}$ for a tidal flare (Ulmer 1999). However, the flare may have been observed significantly past its peak or could be the result of a “weak” encounter that stripped the outer layers of the stellar atmosphere. Our ability to estimate the flare’s bolometric luminosity (L_{bol}) is also limited by the spectral response of ACIS-I below $\sim 0.5 \text{ keV}$. If the spectrum is better described as a steep absorbed power law or multi-

temperature blackbody, L_{bol} could be an order of magnitude or more greater than L_X .

We thus find a tidal disruption event located at the center of SDSS J131122.15-012345.6 to be the most likely explanation for the X-ray flare and the following discussion proceeds based on this assumption.

3.4. Comparison of Observations to Tidal Flare Models

With only a few data points we cannot determine the shape of the flare light curve observationally. But by examining the flare’s X-ray light curve and spectral properties, we show here that the flare is consistent with the expected behavior of a tidal disruption event.

3.4.1. Light Curve Decay

Comparison with a Tidal Flare Accretion Model:— At the early times, the mass infall rate \dot{M} for fallback of the stellar debris from a tidal disruption may exceed the Eddington limit \dot{M}_{Edd} , even as the luminosity flare remains near the Eddington luminosity L_{Edd} (e.g. Ulmer 1999). The central UV/X-ray source may also be obscured at the earliest times by optically luminous super-Eddington outflows on a timescale of days (Strubbe & Quataert 2009).

At later times, when $\dot{M} \lesssim \dot{M}_{Edd}$, the luminosity is expected to track the rate of return of stellar debris and the accretion rate onto the black hole with a decline according to $[(t - t_D)/(t_0 - t_D)]^{-n}$ where $n = 5/3$ by theory (Phinney 1989; Evans & Kochanek 1989; Ayal et al. 2000), t_0 is the peak \dot{M} and t_D is the time of disruption.

The observations constrain t_0 between the *XMM-Newton* nondetection at 2001.98 and the *Chandra* high state at 2004.16. Even though there are several archival observations of Abell 1689, the flare was clearly detected at only only two epochs and was barely detectable by 2006.18. Given the short duration and the resulting low level of statistical significance of the 2007.18 observation, we omitted it as a constraint for the purposes of fitting the decay of the light curve and simply solve for t_D analytically with two points. For a time t in years where $t > t_0 > t_D$ and $t_D \sim 2003.40$, we obtain

$$L_X(0.3 - 3 \text{ keV}) = (3.0 \pm 2.9) \times 10^{42} \text{ erg s}^{-1} \times \left[\frac{t - (2003.40 \pm 0.49)}{1 \text{ yr}} \right]^{-5/3}. \quad (1)$$

This relation is shown in Figure 6 with data points, error bars and upper limits included. The expected rise from t_D to t_0 is not indicated but is discussed below. Note the large uncertainty in the normalization is strongly correlated with the uncertainty in t_D .

The variability and spectral shape (see §2.2.2, §2.2.3, and Figs. 2 and 3) of the X-ray data are therefore consistent with the interpretation that we have identified a tidal disruption event, which we will examine in more detail as follows.

Dynamical Interpretation:— By examining plausible values for the dynamical timescale of the disruption, we place constraints on both the time of disruption and the properties of the disrupted star. Theoretically, the difference between t_D and t_0 should be governed by the specific energy of the stellar material falling back to the

black hole, such as is calculated by Li et al. (2002) as follows. Let R_* and M_* be the radius and mass of the disrupted star, R_p is its periastron and R_t is the tidal radius of the MBH with mass M_\bullet . Then,

$$(t_0 - t_D) = 0.11 \text{ yr } k^{-3/2} \left(\frac{M_\bullet}{10^6 M_\odot} \right)^{1/2} \times \left(\frac{R_p}{R_t} \right)^3 \left(\frac{R_*}{R_\odot} \right)^{3/2} \left(\frac{M_*}{M_\odot} \right)^{-1} (1 + z). \quad (2)$$

We have increased the timescale here according to redshift of the host galaxy, z , as per Gezari et al. (2009). The value of k depends on the extent of the star's spin-up by the tidal encounter, with a minimum of $k = 1$ for a non-rotating star and maximum $k = 3$ for a star that is spun up near the point of break-up. Simulations and linear analysis favor values approaching maximum value, although the full range is possible in principle (Alexander & Kumar 2001; Li et al. 2002).

If $\log(M_\bullet/M_\odot) = 6.46 \pm 0.38$ for the host galaxy, as derived from the $M_\bullet - L$ relationship, then for a main sequence star and $k = 3$,

$$0.02 < (t_0 - t_D) \times (R_p/R_t)^{-3} < 0.06 \text{ yr}. \quad (3)$$

This short dynamical timescale implies $t_0 \ll 2004.16$ for a main sequence star, suggesting the flare is consistent with a tidal disruption event which is already well decayed from its peak when first observed.

The analysis above assumes $M_* \sim M_\odot$ and $R_* \sim R_\odot$, but should also be appropriate for a wide range of plausible stellar masses and radii. Note that $(t_0 - t_D) \propto (M_*/M_\odot)^{-1} (R_*/R_\odot)^{3/2}$, and while it is common to assume a stellar mass-radius relationship $R_* \sim R_\odot (M_*/M_\odot)^{\alpha_R}$ where $\alpha_R = 1$ for main-sequence stars of $M_* < 1 M_\odot$ (e.g. Li et al. 2002), $\alpha_R \sim 0.75$ is empirically appropriate for main sequence stars of $M_* > 1$ (Hansen et al. 2004). Above $M_* = 1 M_\odot$, $(t_0 - t_D)$ depends only weakly on increasing stellar mass. This includes the characteristic properties of luminous S-stars such as dominate observations of our own galactic center (Alexander 2005) and are therefore of great interest as plausible tidal disruption progenitors.

Suppose an alternative interpretation that does not presuppose unobserved early peak emission, such that $t_0 \sim 2004.16$. Such a scenario would be possible if the disrupted star had a large radius, such as a giant, facilitating very long decay timescales (e.g. Lodato et al. 2009). The disruption of a giant is plausible given that observations of our own galaxy have demonstrated the presence of numerous early-type giants, as well as a depleted population of late-type giants, within ~ 0.1 pc of Sag A* (e.g. Do et al. 2009).

In summary, we find that the dynamical time scale of the light curve implies a flare significantly decayed from its peak luminosity or that the disrupted star was a giant. The data do not allow us to distinguish between these two possibilities.

3.4.2. Accreted Mass

To further examine the properties of the disrupted progenitor, we estimate the total X-ray energy released by

integrating the luminosity over the duration of the flare. The total mass accreted is thus

$$\Delta M = \frac{\Delta E}{\epsilon c^2} = \frac{f_{bol}}{\epsilon c^2} \int_t^\infty L_X(t) dt, \quad (4)$$

where $\epsilon \sim 0.1$ and f_{bol} is the bolometric correction (here ~ 1.4). We derived the bolometric correction by taking the ratio of luminosities over 0.3–3 keV and over all significantly contributing energies as derived through numerical integration of a 0.12 keV blackbody, for which the peak photon energy ~ 0.6 keV. The bolometric correction could in principle be an order of magnitude larger, however, if instead the X-ray emission arises from a steep absorbed power law or multi-temperature blackbody (e.g. Gezari et al. 2009; Strubbe & Quataert 2009).

For a lower bound on t , we could conservatively use observed luminosity in the high state as the peak of flare, which is only $\sim 1\%$ of the Eddington Luminosity $L_{Edd} = 1.3 \times 10^{45} (M_\bullet/10^7 M_\odot) \text{ erg s}^{-1}$. This gives $\Delta M > 1.3 \times 10^{-3} M_\odot$ after the date of peak observed luminosity. But if $0.02 < (t_0 - t_D) < 0.06 \text{ yr}$, as predicted from the host galaxy and the $M_\bullet - \sigma$ relation, then $\Delta M \sim 0.01 M_\odot$ total, such that $M_* \gtrsim 0.1 M_\odot$ for a mass accretion fraction of 0.1. A wide variety of conditions could produce modest accretion from a more massive star. Such scenarios include partial stripping of a star's outer layers or tidal detonation due to a strong counter (Carter & Luminet 1982; Brassart & Luminet 2008; Esquej et al. 2008). The range of plausibly accreted masses is therefore consistent with the mass range derived in the previous section.

3.4.3. Geometry of Emission

Finally, we use the X-ray spectral properties to address the plausibility of an emission region described by a disk formed by the accretion of tidal debris.

Following Li et al. (2002), we can estimate a characteristic radius (R_X) of the region emitting X-rays by requiring the blackbody radiation arise from a projected disk and assuming a correction factor $f_c = 3$ to the blackbody temperature T_{bb} to account for spectral hardening by comptonization. We thus find

$$R_X = \left(\frac{f_{bol} f_c^4 L_X}{\pi \sigma T_{bb}^4} \right)^{1/2}. \quad (5)$$

By this calculation, $R_X = 1.3 \pm 0.4 \times 10^{12} \text{ cm}$. For comparison, the Schwarzschild radius of a black hole $R_S \sim 3 \times 10^{12} (M_\bullet/10^7 M_\odot) \text{ cm}$. With only ~ 30 source counts, the flare data do not warrant detailed accretion disk modeling. But to first approximation we see that the area of emission is comparable to the estimated size of the host galaxy black hole, $R_S \sim 8.6 \times 10^{11} \text{ cm}$.

If we assume the X-rays trace the innermost edge of an accretion disk, our estimated range of M_\bullet from the host galaxy also corresponds roughly to a range of innermost stable circular orbits (ISCO) for physically permissible black hole spins a , such that $0.62 \lesssim R_X/R_S \lesssim 3.6$ (compared to $0.5 < R_{ISCO}/R_S < 3$ for $1 > a > 0$, see for example Shapiro & Teukolsky 1986).

3.4.4. Summary of Model-Data Comparisons

The spectral properties and light curve of the flare are consistent with those predicted for a tidal disruption event of a star by a black hole with M_\bullet predicted by the M_\bullet – L relationship. If described by the characteristic $t^{-5/3}$ decay of a tidal flare, the baseline dynamical timescale of the galaxy’s central black hole implies either a disrupted main sequence star that has decayed significantly from its peak luminosity by the time of the observed high state, or a giant star that may instead be near to its peak. By integrating the light curve of the flare, we find that reasonable assumptions of mass accretion rates and efficiency are compatible with the disruption of a star where $M_* \gtrsim 0.1 M_\odot$. And a blackbody model for the observed spectrum predicts a region of emission consistent with an accretion disk, whose inner edge can be described by the ISCO over a plausible range of M_\bullet and black hole spin a .

4. TIDAL DISRUPTION RATE FROM ABELL 1689

A comprehensive estimate of the disruption rate per galaxy per year is complicated by the nonuniformity of the X-ray field coverage, observation spacing, limiting flux as a function of position the expected number of galaxies within the X-ray fields of view, and the expected black hole mass function for different observed host galaxy types. A straightforward method of estimating the rate is to assume that a given number of events N_t is characteristic of the number of galaxies observed N_{gal} and the timespan τ over which the observations are sensitive to tidal flare emission. Let the rate per galaxy per year then simply be $\gamma = N_t/(N_{gal}\tau)$.

We will first proceed with the conservative assumption that the SDSS J131122.15-012345.6 flare is the only true tidal flare. This assumption effectively gives us a “best estimate” for the flare rate such that $N_t = 1$. We can estimate the limits of τ to which our observations are sensitive from the limiting flux of the observations for a given black hole mass. Assuming $z = 0.19$, we can use the theoretical decay of flare accretion as described by Li et al. (2002) to solve for

$$\tau \sim (t - t_D) \sim \left(\frac{F_{-13}}{1.5} \right)^{-3/5} \left(\frac{M_\bullet}{10^7 M_\odot} \right)^{3/5} \text{ yr}, \quad (6)$$

where F_{-13} is the limiting flux of the observation in terms of $10^{-13} \text{ erg cm}^{-2} \text{ s}^{-1}$.

Due to the diffuse X-ray emission of the cluster, the limiting flux is dependent on the distance from the cluster center, where the number of galaxies per unit solid angle is greatest. We must thus consider the impact of the ICM in our estimation of N_{gal} and τ . To calculate our sensitivity, we therefore exclusively use values for the S band (0.3–2.5 keV). This selection minimizes the hard contribution to the background and we expect few or no flare photons at higher energies, whereas the ICM contribution at higher energies is likely to be significant. To determine a comprehensive limiting flux, we select a minimum of $L_X(0.3\text{--}2.5 \text{ keV}) = 10^{42} \text{ erg s}^{-1}$ for a tidal flare high state to differentiate from Ultra-Luminous X-ray sources (ULXs; e.g., Heil et al. 2009) and other similarly luminous sources, and assume $kT_{bb} \sim 0.12 \text{ keV}$ as observed. This selection criterion also sets a strong lower limit to M_\bullet for any flares in our sample, given

$L_{Edd} \gtrsim 10^{42} \text{ erg s}^{-1}$ for $M_\bullet \gtrsim 10^4 M_\odot$. The exposure at epoch 2006.18 is sufficiently deep that it is sensitive over the whole field to disruption events beginning as early as the 2001.02 epoch under these selection criteria from flares similar to the SDSS J131122.15-012345.6 flare such that $\sim 3\sigma$ from $M_\bullet \geq 10^6 M_\odot$, except in the central $\sim 1'$ of the cluster. There, X-ray emission is dominated by the ICM.

Observations at earlier *Chandra* epochs (2000.29, 2001.02) are sensitive across the field to $L_X(0.3\text{--}2.5 \text{ keV}) \sim 5 \times 10^{42} \text{ erg s}^{-1}$ at 3σ . Outside of the central $1'$ radius, early *Chandra* epochs are thus sensitive to disruptions from $M_\bullet \sim 10^6 M_\odot$ over time scales of $\sim 1.5 \text{ yr}$. The single *XMM-Newton* epoch at 2001.98 has a broadband (0.1–12.0 keV) 3σ sensitivity $\lesssim 10^{42} \text{ erg s}^{-1}$ across the field.

We can estimate N_{gal} by modeling the number of galaxies observed projected in ACIS-I according to previously determined cluster characteristics. Lenze et al. (2009) found A1689 to have a limiting radius of $2.1 h^{-1} \text{ Mpc}$ assuming $z=0.183$ and a maximum radial velocity amplitude of $\sim |4000| \text{ km s}^{-1}$ at $300 h^{-1} \text{ kpc}$. We use the surface number density as a function of radius that they determined, namely $\Sigma_n = \Sigma_0/[1 + (r/r_c)^2]^p + C$ where $\Sigma_0 \sim 1300 \text{ galaxies } h^{-2} \text{ Mpc}^{-2}$, $r_c \sim 395 h^{-1} \text{ kpc}$, $p \sim 1$ and C is the number of background galaxies. We estimate that a given *Chandra* field of view with all four ACIS-I chips active plus ACIS-S6 contains $N_{gal} \sim 2100$ cluster members to a depth of $I_{AB} = 26.5$, eight magnitudes fainter than the characteristic bend at luminosity L^* in the cluster luminosity function (e.g. Paolillo et al. 2001), and only $\sim 0.1 N_{gal}$ will be found in the central $1'$ of bright ICM emission. Since fewer than $\sim 10\%$ of the galaxies covered by our observations are close enough to the cluster core to be effectively obscured by the ICM, the bright diffuse background from this region will therefore have only minor effects on the overall estimated rate and hence can be ignored.

If, from the M_\bullet – L relation, we assume our candidate flare represents a characteristic $M_\bullet \sim 3 \times 10^6 M_\odot$, then the ~ 7 years of X-ray observations for A1689 imply we are sensitive to tidal flares of similar luminosity and duration for at least $\tau \sim 8$ years. Combined with $N_{gal} \sim 2100$, this yields $\gamma \sim 6 \times 10^{-5} \text{ galaxy}^{-1} \text{ yr}^{-1}$ for all galaxies in the sample. Without taking effects of the galaxy population composition into account, this is in excess of $\sim 10^{-5}$ as found by Donley et al. (2002), within the bounds set by Luo et al. (2008), and a factor of ~ 4 less than estimated by Esquej et al. (2008). Esquej et al. (2008) used the Ferrarese & Ford (2005) M_\bullet – σ relationship and the Wang & Merritt (2004) rate predictions such that $\gamma \sim 7.0 (M_\bullet/10^6 M_\odot)^{-0.28} \times 10^{-4} \text{ galaxy}^{-1} \text{ yr}^{-1}$. For an assumed $M_\bullet \sim 2.88 \times 10^6 M_\odot$, the same formulation predicts $\gamma = 5.2 \times 10^{-4} \text{ galaxy}^{-1} \text{ yr}^{-1}$, a factor of 9 greater than the rate we calculated above for A1689.

However, since we expect that lower values of M_\bullet will have markedly shorter durations based on strength and rate of decay, suppose that for $M_\bullet \sim 3 \times 10^6 M_\odot$, the observable rate will likely be dominated by black holes of M_\bullet within an order of magnitude. We can estimate the contributing fraction of the cluster population by integrating a Schechter (1976) luminosity function. We

use $K_s = 17.02$ as above (Stanford et al. 2002) and a K_s -band function as determined by King et al. (2002), such that $\alpha = -1.01$ and $m_* = 14.6$. Marconi & Hunt (2003) determine an $M_\bullet - L_K$ relationship such that $\log_{10} M_\bullet \propto -2.2K$ and there is little variation in $M_\bullet - L$ relationships across several near-infrared bands. We integrate the Schechter function over $K_s \pm 2.2$, and then compare that value to the full galaxy population which is integrated down to $m_* + 8$ (analogously to the I_{AB} limiting sensitivity determined by Lemze et al. (2009)), or $M_* + 8 = -16.8$ with K-corrections from King et al. (2002). We thus find $\sim 49\%$ of the galaxies to be likely contributors to the production of flares detectable by our observations. If, therefore, $N_{gal} \approx 0.49 \times 2100 \approx 1000$, the disruption rate we infer from a *single* event is 1.2×10^{-4} . This rate is within a factor of two of the Esquej et al. (2008) rate that makes no corrections for nondetections of flares in heavily absorbed edge-on spirals.

But suppose that tidal flares account for some significant fraction of the other sources we detected that both displayed significant X-ray variability and could not be unambiguously eliminated from consideration. The highest upper bound for the flare rate would include all 14 objects as potential tidal flares. This bound is too high as we can exclude all of the SDSS-matched objects as likely AGNs or stars based upon the optical properties previously described. According to Ivezić et al. (2002), SDSS morphological classification is robust to 95% as faint as $r \sim 21.5$, suggesting the matched stellar objects (all of comparable magnitude or brighter) are unlikely to be misclassified galaxies. And a tidal optical flare of the type predicted by Strubbe & Quataert (2009) ($\nu L_\nu \sim 10^{41}$ erg s $^{-1}$ in g) is too faint to be detected by SDSS at $z \sim 0.19$, so that such a flare could not explain starlike unresolved optical emission from a cluster member.

Removing these 7 SDSS-matched objects from our sample, we are left with 7 remaining unmatched variable sources that lack optical identifications and are outside the FOV of all HST observations of A1689. These objects could be background AGN that are optically fainter than the SDSS *ugriz* limiting magnitudes. We will now calculate upper limits to the flare rate as determined from two alternate cases that do not ignore these unmatched X-ray sources. In the first case, we assume that all of these variable sources are cluster members. In the second case we attempt to estimate what fraction of these unmatched sources are line-of-sight objects rather than cluster members. But in either of these cases, any host galaxy within the cluster would have to be a dwarf galaxy. With the Lupton (2005) magnitude conversions and the Lauer et al. (2007) $M_\bullet - \sigma$ relation, the SDSS g and r limiting magnitudes suggest dwarf host galaxies are unlikely to have $M_\bullet > 10^{5.5} M_\odot$. A flare without an obvious host could also arise from an intracluster MBH ejected during an MBH merger (Komossa & Merritt 2008).

In the first case, under the unlikely assumption that all optically unidentified sources were indeed tidal disruption flares from faint (dwarf) cluster galaxies, the rate for all galaxies would be $\gamma \sim 8.2 \times 10^{-4}$. But if the typical duration of a flare becomes shorter with decreasing M_\bullet , the effective value of $N_{gal}\tau$ will also be less

than if we had assumed uniform flare duration. Suppose we therefore assume a Schechter (1976) profile and $\tau \propto M^{3/5}$ as before, with a power law spectrum $\Gamma = 2$ (using a harder spectral profile like a typical AGN and consistent with the uniform hardness ratio distribution of these objects). Rounding our limit of $M_\bullet \lesssim 10^{5.5} M_\odot$ up to $10^6 M_\odot$ for dwarf galaxies and given the Eddington-limited lower bound of $M_\bullet \gtrsim 10^4 M_\odot$, the integrated $N_{gal}\tau$ for $10^6 M_\odot > M_\bullet > 10^4 M_\odot$ in our dataset is only ~ 1400 galaxy-years. Thus, in this case $\gamma \sim 5.0 \times 10^{-3}$ for the subset of galaxies where $M_\bullet \lesssim 10^6 M_\odot$. This specific rate is several times greater than even the most optimistic values (e.g. $\gamma = 1.2 \times 10^{-3}$ for $M_\bullet = 10^5 M_\odot$ from Wang & Merritt (2004)).

In the second case, we calculate a more plausible disruption rate by using the Lemze et al. (2009) galaxy distribution function to determine the likelihood of any given galaxy being a cluster member rather than a field galaxy. This probability decreases at greater radii from the cluster center. Starting at $r > 800$ kpc from the cluster center, even the most central of these 7 optically unidentified sources would be no more than $\sim 40\%$ likely to be a cluster member. If we consider only the respective projected distances from the cluster center for a set of unknown galaxies, there is a 77% chance that at least one of these seven galaxies is a cluster member. The most likely or “expectation” value is $\bar{n} = 1.3$ cluster members. Here $\bar{n} \equiv \sum_{0 \leq i \leq n} p(r_i)$ where $n = 7$ is the number of galaxies and $p(r_i)$ is the probability of galaxy i being a cluster member at radius r_i from the cluster center. The expected number of field galaxies is therefore $n - \bar{n} = 5.3$. This estimate neglects any bias introduced in a dataset selected for X-ray emission and variability.

To determine an upper bound for N_t in this calculation, we consider $\bar{n} \sim 1.3$ optically unidentified X-ray-variable cluster members, plus a tidal flare in SDSS J131122.15-012345.6 and corresponding statistical error of 2.4 based on Gehrels (1986). Therefore $N_t \lesssim 4.7$ and $\gamma \lesssim 4.8 \times 10^{-4}$. These assumptions also indicate $\gamma \lesssim 2.6 \times 10^{-3}$ for $10^6 M_\odot > M_\bullet > 10^4 M_\odot$, which is consistent with the predictions of Wang & Merritt (2004). Thus, our observations do not exclude the possibility that most dwarf galaxies contain MBHs in this mass range.

5. SUMMARY AND CONCLUSIONS

We report an X-ray flare that occurred within a projected distance of 1.6 kpc from the center of the spiral galaxy SDSS J131122.15-012345.6. The projected positional uncertainty is 4.7 kpc. The peak observed luminosity ($L_X(0.3-3$ keV) $\sim 5 \times 10^{42}$ erg s $^{-1}$, assuming it originated from a member of A1689), strong variability ($\times 30$), supersoft spectrum ($kT_{bb} = 0.12$ keV), slow evolution ($\times 9$ decay over ~ 2 years), and absence of strong optical emission lines from the presumed host galaxy ~ 5 years after the outburst are consistent with other existing examples of X-ray flares that have been classified as arising from tidal disruption events. Although we cannot completely rule out another origin for the X-ray flare, we conclude that the most likely explanation is a flare due to the tidal disruption of a star by an MBH. To the best of our knowledge, this is the first reported *Chandra*-selected discovery of such a flare.

Based on observations of a cluster with a well-measured

galaxy population and over a well-defined period of time, we have therefore calculated an event rate of $\sim 10^{-4}$ tidal disruption events galaxy $^{-1}$ yr $^{-1}$ under the assumption that all inactive, non-dwarf galaxies have central black holes of $M_{\bullet} = 10^6 - 10^8 M_{\odot}$ and will produce tidal flares. The calculated event rate is consistent with previously reported theoretical and observational work. Our results coupled with those of Cappelluti et al. (2009) present a strong case for cluster surveys to detect X-ray flares from tidal disruption events. Our work is consistent with the hypothesis that all normal galaxies (such as SDSS J131122.15-012345.6) host massive black holes at their center, but our results do not exclude other models of galaxy formation in which MBHs are rarer or (alternatively) more massive than the $M_{\bullet} - \sigma$ relation implies (e.g. Volonteri et al. 2005).

Determining the rate of tidal flares from lower mass black holes, if they occur at all, has the potential to constrain existing models of dwarf galaxy formation and evolution. A more accurate disruption rate for normal galaxies in clusters compared to rates derived from the field could also be related to galaxy evolution in rich clusters of galaxies. In particular, it could have implications for how galaxy mergers affect black hole mass distribution and stellar populations in galaxy clusters.

Flares from low mass ($M_{\bullet} \lesssim 10^6 M_{\odot}$) black holes may (Wang & Merritt 2004) or may not (Merritt 2009) contribute disproportionately to the overall flaring rate. But if low mass black holes produce tidal flares of shorter observable duration, existing cluster X-ray observations of a typical ~ 2 year cadence could miss tidal flares even for an actual rate that is perhaps a factor of 10 higher. Further dedicated X-ray observations of clusters using *Chandra*, *XMM-Newton* or future soft-sensitive (0.1–3.0 keV) missions with comparable or better fields of view such as *WFXT* (Murray et al. 2008), *IXO* (Parmar 2009) or *eRosita* (Predehl et al. 2007) are therefore necessary, to

find events from less massive central black holes (to the extent that such less massive black holes exist) and to refine the disruption rate per galaxy.

PM and MU acknowledge the support of a NASA ADP grant NNX08AJ35G. PM was also supported in part by the NASA Illinois Space Consortium grant 2005-3386-02 \ NNG05GE81H and GAANN fellowship grant P200A060082. We thank the referee for many very helpful comments. We gratefully acknowledge the support of NASA for continued operations of *HST*, *Chandra* and their data archives, the ESA's support of *XMM-Newton* and its archives and the continued efforts of the Sloan Digital Sky Survey. We are grateful to Dirk Grupe for many useful discussions, and to Vincent LeBrun for fitting the HET spectrum with *EZ*. PM thanks Arnold Rots for his help with the *GLvary* code and Olivier Ilbert for his help with *LePhare*. MU thanks Andrew Ulmer and Marc Freitag for helpful discussions of tidal flares. The Hobby-Eberly Telescope (HET) is a joint project of the University of Texas at Austin, the Pennsylvania State University, Ludwig-Maximilians-Universität München, and Georg-August-Universität Göttingen. The HET is named in honor of its principal benefactors, William P. Hobby and Robert E. Eberly. The Marcario Low-Resolution Spectrograph (LRS) is a joint project of the Hobby-Eberly Telescope partnership and the Instituto de Astronomía de la Universidad Nacional Autónoma de México. This research has made use of the NASA/IPAC Extragalactic Database (NED) which is operated by the Jet Propulsion Laboratory, California Institute of Technology, under contract with the National Aeronautics and Space Administration.

Facilities: CXO(ACIS), XMM, HET, SDSS, HST(WF/PC2).

REFERENCES

- Adelman-McCarthy, J. K., et al. 2008, *ApJS*, 175, 297
 Alexander, T. 2005, *Physics Reports*, 419, 65
 Alexander, T., & Kumar, P. 2001, *ApJ*, 549, 948
 Amaro-Seoane, P., Gair, J. R., Freitag, M., Miller, M. C., Mandel, I., Cutler, C. J., & Babak, S. 2007, *Classical and Quantum Gravity*, 24, 113
 Andersson, K. E., & Madejski, G. M. 2004, *ApJ*, 607, 190
 Arnaud, K. A. 1996, in *Astronomical Society of the Pacific Conference Series*, Vol. 101, *Astronomical Data Analysis Software and Systems V*, ed. G. H. Jacoby & J. Barnes, 17–20
 Ayal, S., Livio, M., & Piran, T. 2000, *ApJ*, 545, 772
 Bade, N., Komossa, S., & Dahlem, M. 1996, *A&A*, 309, L35
 Barth, A. J. 2001, in *Astronomical Society of the Pacific Conference Series*, Vol. 238, *Astronomical Data Analysis Software and Systems X*, ed. F. R. Harnden, Jr., F. A. Primini, & H. E. Payne, 385–387
 Beckmann, V., Gehrels, N., Shrader, C. R., & Soldi, S. 2006, *ApJ*, 638, 642
 Blanton, M. R., et al. 2003, *ApJ*, 594, 186
 Bogdanović, T., Eracleous, M., Mahadevan, S., Sigurdsson, S., & Laguna, P. 2004, *ApJ*, 610, 707
 Boller, T., Brandt, W. N., Fabian, A. C., & Fink, H. H. 1997, *MNRAS*, 289, 393
 Boller, T., Truemper, J., Molendi, S., Fink, H., Schaeidt, S., Caulet, A., & Dennefeld, M. 1993, *A&A*, 279, 53
 Brandt, W. N., Pounds, K. A., & Fink, H. 1995, *MNRAS*, 273, L47
 Brassart, M., & Luminet, J. 2008, *A&A*, 481, 259
 Campana, S., et al. 2006, *Nature*, 442, 1008
 Cappelluti, N., et al. 2009, *A&A*, 495, L9
 Carter, B., & Luminet, J. P. 1982, *Nature*, 296, 211
 Churazov, E., Gilfanov, M., Forman, W., & Jones, C. 1996, *ApJ*, 471, 673
 Collister, A. A., & Lahav, O. 2004, *PASP*, 116, 345
 Dickey, J. M., & Lockman, F. J. 1990, *ARA&A*, 28, 215
 Do, T., Ghez, A. M., Morris, M. R., Lu, J. R., Matthews, K., Yelda, S., & Larkin, J. 2009, *ApJ*, 703, 1323
 Donley, J. L., Brandt, W. N., Eracleous, M., & Boller, T. 2002, *AJ*, 124, 1308
 Dorman, B., & Arnaud, K. A. 2001, in *Astronomical Society of the Pacific Conference Series*, Vol. 238, *Astronomical Data Analysis Software and Systems X*, ed. F. R. Harnden Jr., F. A. Primini, & H. E. Payne, 415–418
 Duc, P.-A., et al. 2002, *A&A*, 382, 60
 Elvis, M., et al. 1994, *ApJS*, 95, 1
 Esquej, P., Saxton, R. D., Freyberg, M. J., Read, A. M., Altieri, B., Sanchez-Portal, M., & Hasinger, G. 2007, *A&A*, 462, L49
 Esquej, P., et al. 2008, *A&A*, 489, 543
 Estrada, J., et al. 2007, *ApJ*, 660, 1176
 Evans, C. R., & Kochanek, C. S. 1989, *ApJ Lett.*, 346, L13
 Feigelson, E. D., Broos, P., Gaffney, III, J. A., Garmire, G., Hillenbrand, L. A., Pravdo, S. H., Townsley, L., & Tsuboi, Y. 2002, *ApJ*, 574, 258
 Ferrarese, L., & Ford, H. 2005, *Space Science Reviews*, 116, 523
 Ferrarese, L., et al. 2006, *ApJ*, 644, L21

- Fruscione, A., et al. 2006, in Society of Photo-Optical Instrumentation Engineers (SPIE) Conference Series, Vol. 6270, Society of Photo-Optical Instrumentation Engineers (SPIE) Conference Series
- Gehrels, N. 1986, *ApJ*, 303, 336
- Genzel, R., et al. 2003, *ApJ*, 594, 812
- Gezari, S., Halpern, J. P., Komossa, S., Grupe, D., & Leighly, K. M. 2003, *ApJ*, 592, 42
- Gezari, S., et al. 2006, *ApJ*, 653, L25
- . 2008a, *ApJ*, 683, L131
- . 2008b, *ApJ*, 676, 944
- . 2009, *ApJ*, 698, 1367
- Ghez, A. M., Becklin, E., Duchjné, G., Hornstein, S., Morris, M., Salim, S., & Tanner, A. 2003, *Astronomische Nachrichten Supplement*, 324, 527
- Giacconi, R., et al. 2001, *ApJ*, 551, 624
- Graham, A. W., & Driver, S. P. 2005, *Publications of the Astronomical Society of Australia*, 22, 118
- Greene, J. E., Ho, L. C., & Barth, A. J. 2008, *ApJ*, 688, 159
- Gregory, P. C., & Loredo, T. J. 1992, *ApJ*, 398, 146
- Grupe, D. 2004, *AJ*, 127, 1799
- Grupe, D., Beuerman, K., Mannheim, K., Thomas, H., Fink, H. H., & de Martino, D. 1995a, *A&A*, 300, L21+
- Grupe, D., Beuermann, K., Mannheim, K., Bade, N., Thomas, H., de Martino, D., & Schwöpe, A. 1995b, *A&A*, 299, L5+
- Grupe, D., Komossa, S., Gallo, L. C., Fabian, A. C., Larsson, J., Pradhan, A. K., Xu, D., & Miniutti, G. 2008a, *ApJ*, 681, 982
- Grupe, D., Leighly, K. M., & Komossa, S. 2008b, *AJ*, 136, 2343
- Grupe, D., Thomas, H., & Leighly, K. M. 1999, *A&A*, 350, L31
- Grupe, D., Wills, B. J., Leighly, K. M., & Meusinger, H. 2004, *AJ*, 127, 156
- Grupe, D., et al. 2010, *ApJ*, 711, 1008
- Halkola, A., Seitz, S., & Pannella, M. 2006, *MNRAS*, 372, 1425
- Halpern, J. P., Gezari, S., & Komossa, S. 2004, *ApJ*, 604, 572
- Hansen, C. J., Kawaler, S. D., & Trimble, V. 2004, *Stellar interiors: physical principles, structure, and evolution*, ed. C. J. Hansen, S. D. Kawaler, & V. Trimble
- Heil, L. M., Vaughan, S., & Roberts, T. P. 2009, *MNRAS*, 397, 1061
- Heinke, C. O., Grindlay, J. E., Lugger, P. M., Cohn, H. N., Edmonds, P. D., Lloyd, D. A., & Cool, A. M. 2003, *ApJ*, 598, 501
- Ilbert, O., et al. 2006, *A&A*, 457, 841
- Immler, S., & Lewin, W. H. G. 2003, in *Lecture Notes in Physics*, Berlin Springer Verlag, Vol. 598, *Supernovae and Gamma-Ray Bursters*, ed. K. Weiler, 91–111
- Immler, S., et al. 2008, *ApJ*, 674, L85
- Ivezić, Ž., et al. 2002, *AJ*, 124, 2364
- Jenkins, L. P., Hornschemeier, A. E., Mobasher, B., Alexander, D. M., & Bauer, F. E. 2007, *ApJ*, 666, 846
- Jennrich, O. 2004, in *Optical Fabrication, Metrology, and Material Advancements for Telescopes*. Edited by Atad-Ettinger, Eli; Dierckx, Philippe. *Proceedings of the SPIE*, Volume 5500, pp. 113–119 (2004), ed. J. Hough & G. H. Sanders, 113–119
- Khokhlov, A., & Melia, F. 1996, *ApJ*, 457, L61
- Khokhlov, A., Novikov, I. D., & Pethick, C. J. 1993, *ApJ*, 418, 181
- Kim, M., et al. 2007, *ApJS*, 169, 401
- King, L. J., Clowe, D. I., Lidman, C., Schneider, P., Erben, T., Kneib, J.-P., & Meylan, G. 2002, *A&A*, 385, L5
- Kobayashi, S., Laguna, P., Phinney, E. S., & Mészáros, P. 2004, *ApJ*, 615, 855
- Komossa, S. 2005, in *Growing Black Holes: Accretion in a Cosmological Context*, ed. A. Merloni, S. Nayakshin, & R. A. Sunyaev, 159–163
- Komossa, S., & Bade, N. 1999, *A&A*, 343, 775
- Komossa, S., & Greiner, J. 1999, *A&A*, 349, L45
- Komossa, S., Halpern, J., Scharrel, N., Hasinger, G., Santos-Lleo, M., & Predehl, P. 2004, *ApJ*, 603, L17
- Komossa, S., & Merritt, D. 2008, *ApJ*, 683, L21
- Landman, W. B. 1993, in *Astronomical Society of the Pacific Conference Series*, Vol. 52, *Astronomical Data Analysis Software and Systems II*, ed. R. J. Hanisch, R. J. V. Brissenden, & J. Barnes, 246–248
- Lauer, T. R., et al. 2007, *ApJ*, 662, 808
- Le Fèvre, O., et al. 2005, *A&A*, 439, 877
- Lemze, D., Broadhurst, T., Rephaeli, Y., Barkana, R., & Umetsu, K. 2009, *ApJ*, 701, 1336
- Li, L., Narayan, R., & Menou, K. 2002, *ApJ*, 576, 753
- Lodato, G., King, A. R., & Pringle, J. E. 2009, *MNRAS*, 392, 332
- Loeb, A., & Ulmer, A. 1997, *ApJ*, 489, 573
- Luo, B., Brandt, W. N., Steffen, A. T., & Bauer, F. E. 2008, *ApJ*, 674, 122
- Lupton, R. 2005, *SDSS Photometric Equations*, Batavia, IL: SDSS, <http://www.sdss.org/sdr6/algorithms/sdssUBVRITransform.html>
- Magorrian, J., & Tremaine, S. 1999, *MNRAS*, 309, 447
- Magorrian, J., et al. 1998, *AJ*, 115, 2285
- Marconi, A., & Hunt, L. K. 2003, *ApJ*, 589, L21
- Marconi, A., Risaliti, G., Gilli, R., Hunt, L. K., Maiolino, R., & Salvati, M. 2004, *MNRAS*, 351, 169
- Martini, P., Mulchaey, J. S., & Kelson, D. D. 2007, *ApJ*, 664, 761
- Mathur, S., & Grupe, D. 2005, *ApJ*, 633, 688
- McHardy, I. M., Papadakis, I. E., Uttley, P., Page, M. J., & Mason, K. O. 2004, *MNRAS*, 348, 783
- Merritt, D. 2009, *ApJ*, 694, 959
- Milosavljević, M., Merritt, D., & Ho, L. C. 2006, *ApJ*, 652, 120
- Murray, S. S., et al. 2008, in *Society of Photo-Optical Instrumentation Engineers (SPIE) Conference Series*, Vol. 7011, Society of Photo-Optical Instrumentation Engineers (SPIE) Conference Series
- Paolillo, M., Andreon, S., Longo, G., Puddu, E., Gal, R. R., Scaramella, R., Djorgovski, S. G., & de Carvalho, R. 2001, *A&A*, 367, 59
- Parmar, A. 2009, in *High Resolution X-ray Spectroscopy: Towards IXO*, *Proceedings of the international workshop held at the Mullard Space Science Laboratory of University College London, Holmbury St Mary, Dorking, Surrey, UK, March 19 - 20, 2009*, Ed.s Branduardi-Raymont, G. and Blustin, A., published electronically at <http://www.mssl.ucl.ac.uk/~ajb/workshop3/index.html>, p.E32
- Phinney, E. S. 1989, in *IAU Symp. 136: The Center of the Galaxy*, ed. M. Morris, Vol. 136, 543
- Predehl, P., et al. 2007, in *Society of Photo-Optical Instrumentation Engineers (SPIE) Conference Series*, Vol. 6686, Society of Photo-Optical Instrumentation Engineers (SPIE) Conference Series
- Rees, M. J. 1988, *Nature*, 333, 523
- ROSAT Consortium. 2000, *VizieR Online Data Catalog*, 9030, 0
- ROSAT Scientific Team. 2000, *VizieR Online Data Catalog*, 9028, 0
- Rots, A. H. 2006, in *Astronomical Society of the Pacific Conference Series*, Vol. 351, *Astronomical Data Analysis Software and Systems XV*, ed. C. Gabriel, C. Arviset, D. Ponz, & S. Enrique, 73
- Schechter, P. 1976, *ApJ*, 203, 297
- Schlegel, E. M., & Petre, R. 2006, *ApJ*, 646, 378
- Sérsic, J. L. 1963, *Boletín de la Asociación Argentina de Astronomía La Plata Argentina*, 6, 41
- Sesana, A., Haardt, F., Madau, P., & Volonteri, M. 2004, *ApJ*, 611, 623
- . 2005, *ApJ*, 623, 23
- Shapiro, S. L., & Teukolsky, S. A. 1986, *Black Holes, White Dwarfs and Neutron Stars: The Physics of Compact Objects*, ed. Shapiro, S. L. & Teukolsky, S. A.
- Sigurdsson, S. 2003, *Classical and Quantum Gravity*, 20, 45
- Soderberg, A. M., et al. 2008, *Nature*, 453, 469
- Stanford, S. A., Eisenhardt, P. R., Dickinson, M., Holden, B. P., & De Propriis, R. 2002, *ApJS*, 142, 153
- Strubbe, L. E., & Quataert, E. 2009, *MNRAS*, 400, 2070
- Struble, M. F., & Rood, H. J. 1999, *ApJS*, 125, 35
- Szokoly, G. P., et al. 2004, *ApJS*, 155, 271
- Ulmer, A. 1999, *ApJ*, 514, 180
- Urry, C. M., & Padovani, P. 1995, *PASP*, 107, 803
- Volonteri, M., Madau, P., Quataert, E., & Rees, M. J. 2005, *ApJ*, 620, 69
- Wang, J., & Merritt, D. 2004, *ApJ*, 600, 149
- White, R. L., Becker, R. H., Helfand, D. J., & Gregg, M. D. 1997, *ApJ*, 475, 479
- Wright, E. L. 2006, *PASP*, 118, 1711
- Yanny, B., et al. 2009, *AJ*, 137, 4377
- Zacharias, N., Monet, D. G., Levine, S. E., Urban, S. E., Gaume, R., & Wycoff, G. L. 2005, *VizieR Online Data Catalog*, 1297, 0

Zhou, H., Wang, T., Yuan, W., Lu, H., Dong, X., Wang, J., & Lu,
Y. 2006, ApJS, 166, 128

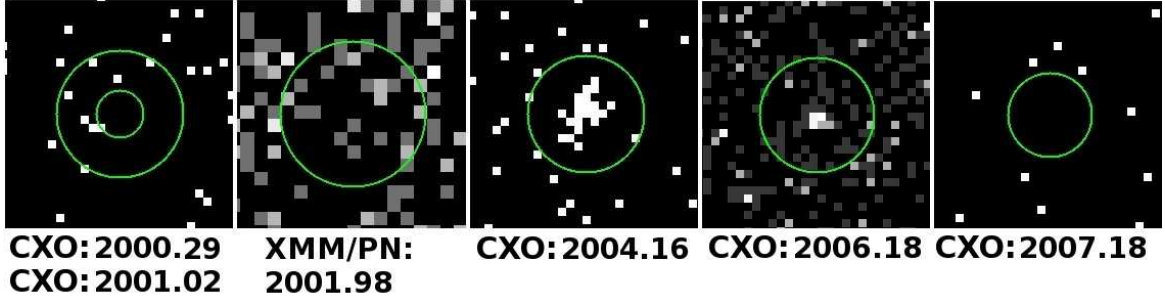


FIG. 1.— Images of the event at the times of observation epochs, starting from pre-flare. Instruments used are indicated: CXO for *Chandra X-ray Observatory* ACIS, and XMM/PN for the *XMM-Newton* PN. Numbers correspond to the date of observation. Circles describe a 95% encircled energy radius for *Chandra* ACIS or 50 in the case of *XMM-Newton* PN. Color scales are uniform and scaled to provide a good contrast at epoch 2006.18. Note that this saturates the color scale at epoch 2004.16, the observation nearest to peak. *Chandra* images are binned from (0.3–10 keV) event files by a factor of two, *XMM-Newton* unfiltered by energy and binned by a factor of 32. Pre-flare *Chandra* epochs have been merged with extraction circles from both epochs indicated (as per differing off-axis angles).

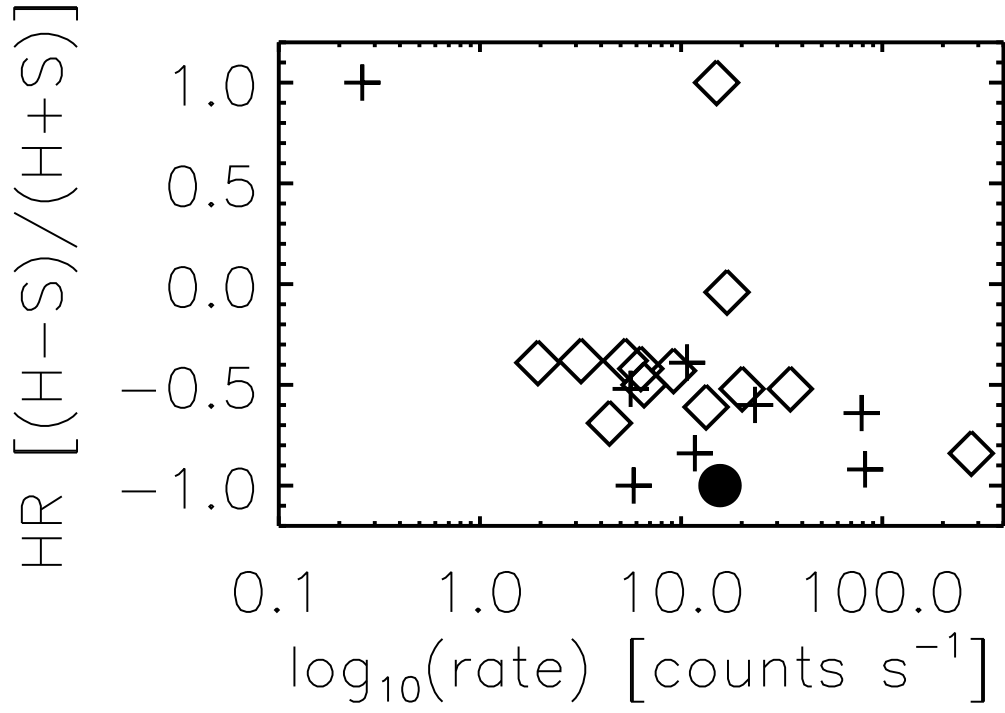


FIG. 2.— Sources from Table. 2 with hardness ratios plotted against corresponding peak count rates. The filled circle indicates our tidal flare candidate, source 141. Crosses mark those X-ray sources which correspond to SDSS objects designated as stars. Diamonds indicate sources all other sources.

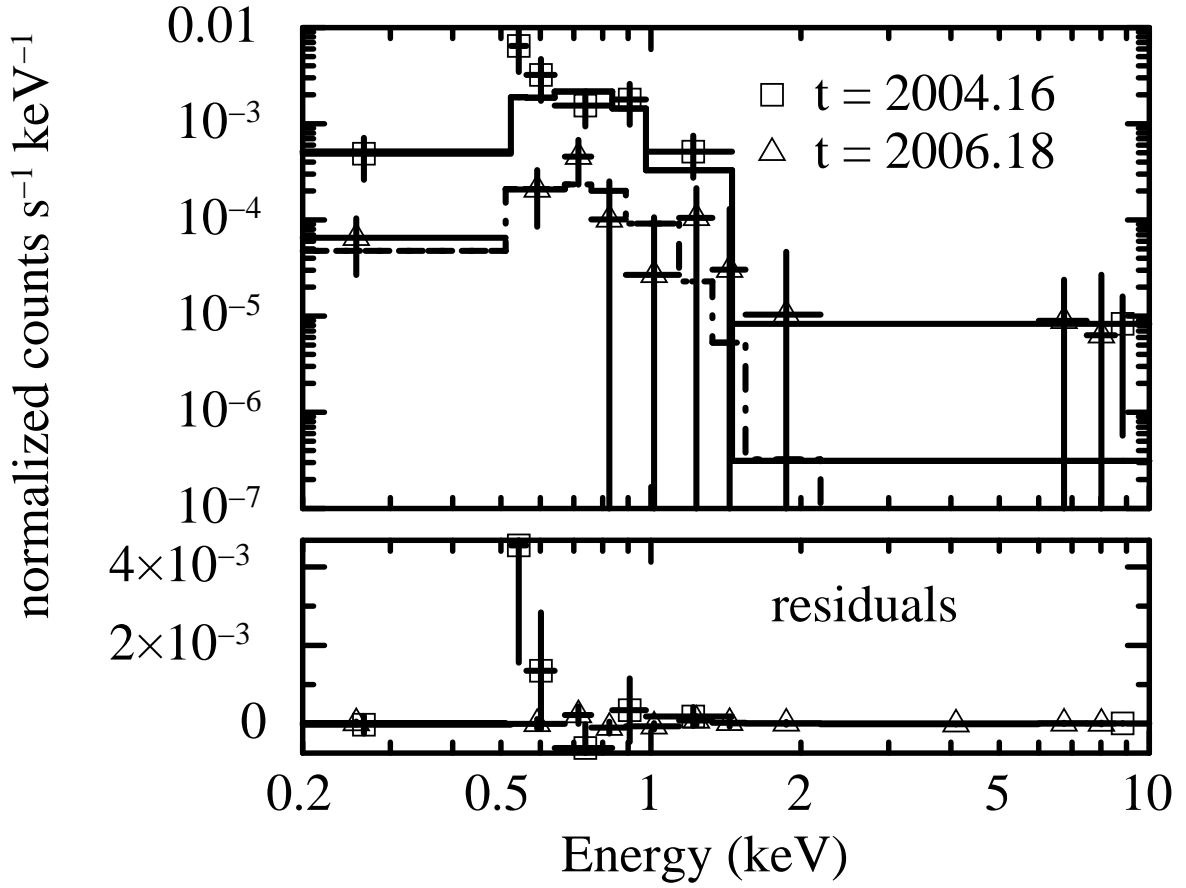


FIG. 3.— Top: fits to the *Chandra* spectra using a $kT = 0.12$ keV blackbody model at the cluster redshift at epochs 2004.16 (solid line: model, squares: data) and 2006.18 (dot-dashed line: model, triangles: data). 1σ errors are indicated. Each bin signifies 5 photon counts. Bottom: residuals between model and data, as above.

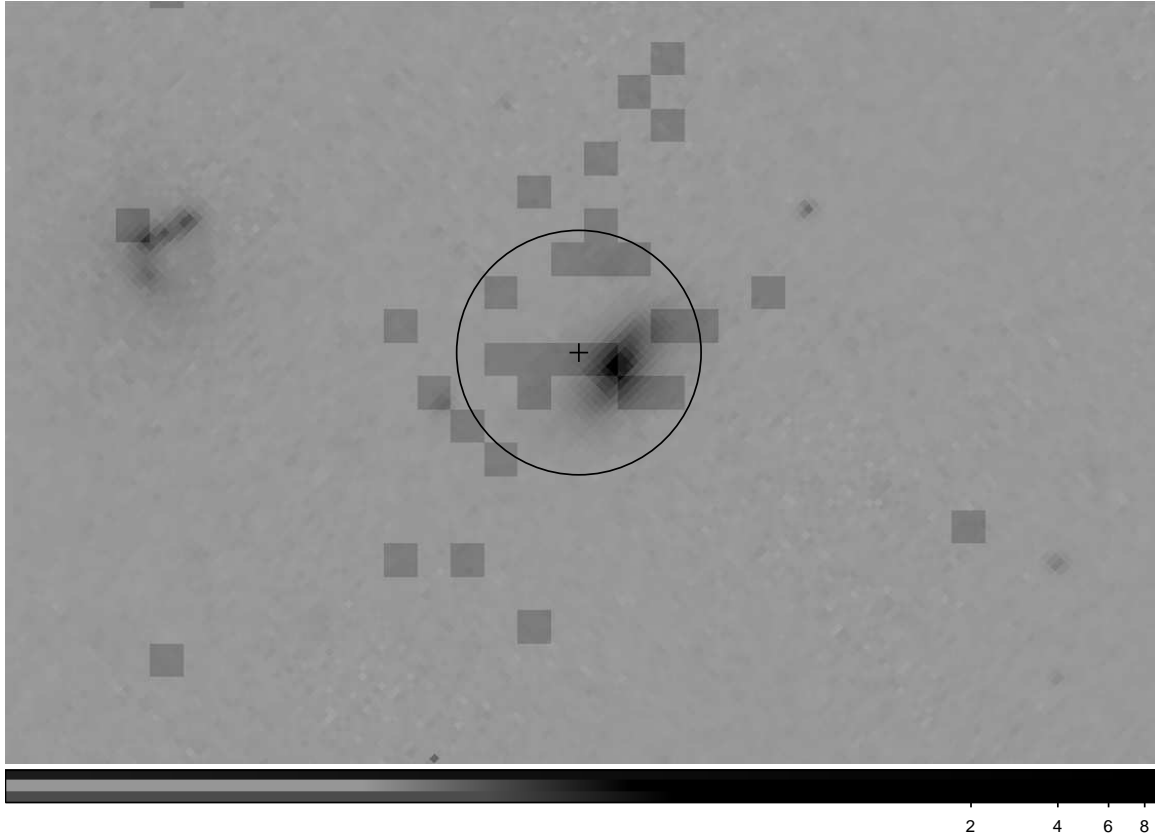


FIG. 4.— Pre-flare HST WFPC2 image of SDSS J131122.15-012345.6 taken using the F606W filter. The larger overlaid pixels are singly binned X-ray events from the flare at its peak at epoch 2004.16. The circle indicates centroid error at $r \sim 1''.8$ and the cross is the middle of the centroid.

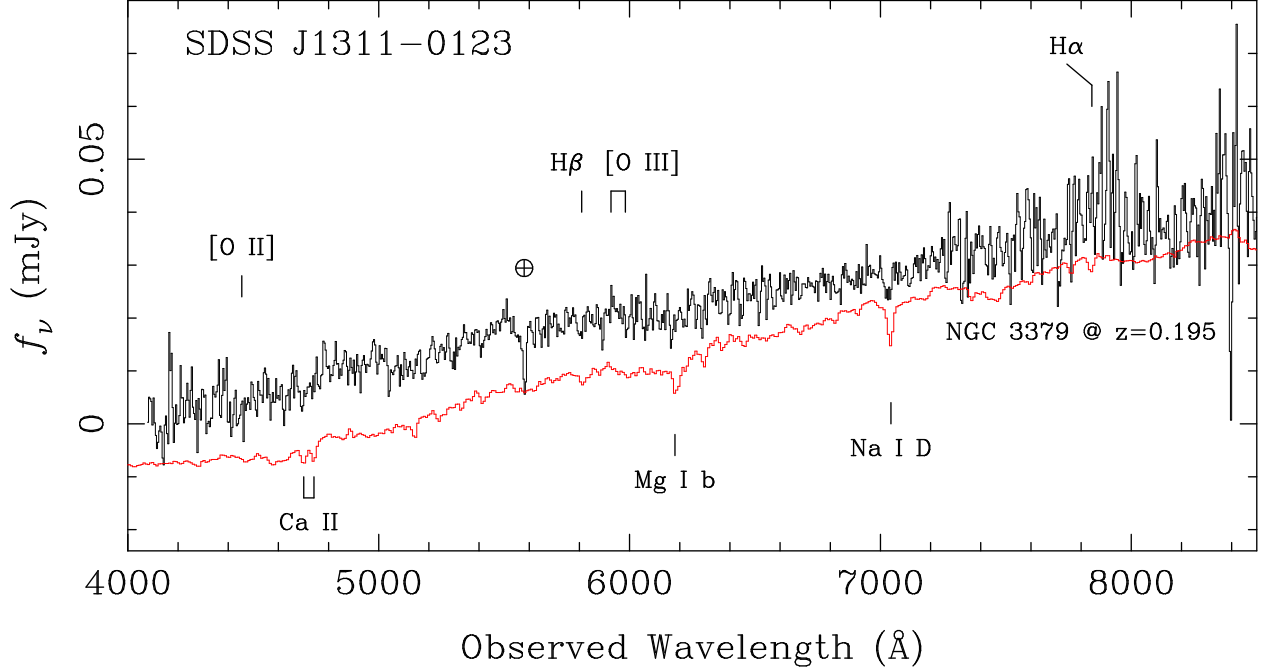


FIG. 5.— Observed *HET* spectrum of the flaring galaxy with a spectrum of the nearby elliptical galaxy NGC 3379 shifted to $z = 0.195$ overlaid for comparison. There is a residual from the imperfect subtraction of the sharp [O I] telluric line at 5577\AA , marked with a crossed circle. In addition, there are also large residuals from poor sky subtraction at wavelengths longer than 7500\AA . Amongst the galaxy's absorption features, at 7000\AA we see the Na I D interstellar line, at 4650\AA are Ca II H and K, and at 6200\AA is Mg I b. The spectrum near H α is dominated by noise from sky subtraction residuals. Note the lack of strong emission lines that would indicate a typical AGN.

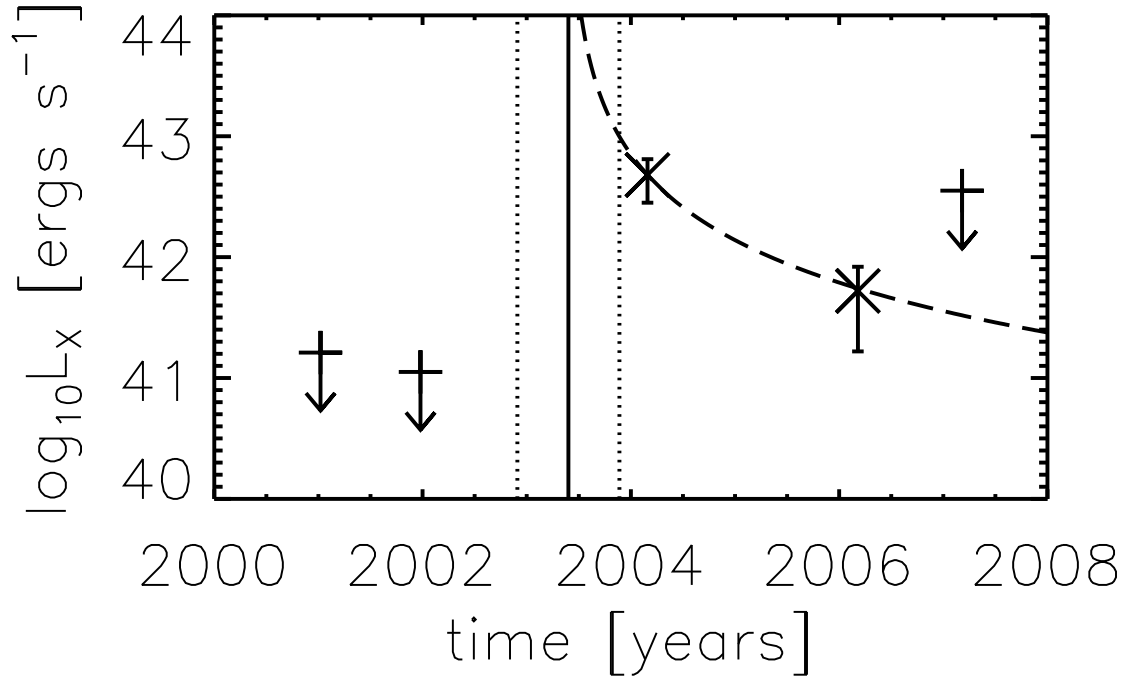


FIG. 6.— Light curve for the flare with error bars. Arrows indicate upper bounds. $L_X(0.3-3)$ corrected for galactic extinction are indicated by \times . The dashed line is a $t^{-5/3}$ light curve which assumes t_D at the expected value for a solar-type star, indicated by the solid vertical line. Dotted lines indicate the error range for t_D . The rise in luminosity between t_D and t_0 is not indicated, nor is the peak luminosity at t_0 shown.

TABLE 1
X-RAY OBSERVATIONS.

Instrument	Obsid	Observation Date (UT)	Duration (ks)	Aim Point Coordinates		Roll Angle
				$\alpha(2000)$	$\delta(2000)$	
ACIS-I	540	2000 Apr. 15	10.5	13:11:13.88	−01:20:14.75	214.302
ACIS-I	1663	2001 Jan. 7	10.5	13:11:34.90	−01:17:10.88	67.828
EPIC	0093030101	2001 Dec. 24	39.8	13:11:33.69	−01:20:29.70	115.755
ACIS-I	5004	2004 Feb. 28	19.9	13:11:33.30	−01:17:20.91	75.154
ACIS-I	6930	2006 Mar. 6	76.9	13:11:32.87	−01:17:21.16	77.129
ACIS-I	7289	2006 Mar. 9	75.7	13:11:32.87	−01:17:21.17	77.129
ACIS-I	7701	2007 Mar. 7	5.1	13:11:37.04	−01:19:13.76	77.454

TABLE 2
VARIABLE SOURCES

Source	RA ($^{\circ}$)	Dec ($^{\circ}$)	SDSS Optical ID	I_{AB}	Chandra Obsid Coverage						Peak Rate (10^{-4} ct s $^{-1}$)	Peak HR $\frac{H-S}{H+S}$	Peak θ ($'$)	Flags
					540	1663	5004	6930	7289	7701				
14	197.9353	-1.1661	none			X	X	P	X		3.18 ± 1.09	-0.38	12.8	1,2
24	197.9825	-1.1709	J131155.51-011017.7	18.45		P	X	X	X		10.7 ± 4.7	-0.39	8.68	4
27	197.8700	-1.1488	J131128.78-010856.5	21.47		X	X	X	P		1.94 ± 1.00	-0.38	8.49	1,3
31	197.7475	-1.1341	J131059.20-010805.5	20.77		X	X	X	P		5.61 ± 1.47	-0.52	12.5	1,2,4
34	197.7035	-1.1420	J131049.00-010832.4	20.15		X	X	X	P		5.27 ± 1.46	-0.42	14.1	1,2,3
43	197.8888	-1.2866	J131133.28-011712.2	19.71	P	X	X	X	X	X	34.9 ± 7.9	-0.69	5.74	2,3
75	197.8232	-1.2121	J131117.54-011244.5	19.92	X		X	P	X	X	0.26 ± 1.07	1.00	6.00	4
77	198.0102	-1.3321	none			X	P	X	X	X	6.30 ± 2.74	-0.04	7.73	1
78	197.9978	-1.2848	J131159.55-011705.6	14.95		P	X	X	X	X	11.7 ± 5.1	-0.84	6.15	2,4
86	197.9058	-1.4036	none		X	X	X	X	P	X	4.40 ± 1.43	-0.52	6.95	1
123	197.7654	-1.4008	none		P					X	15.0 ± 5.6	-0.61	4.58	2,6
131	197.8080	-1.4281	none		P					X	16.9 ± 5.9	-0.43	5.44	
134	197.8259	-1.2416	J131118.20-011429.8	18.36	X	X	X	X	X	P	277 ± 26	-0.50	6.68	2,3,7,8
141	197.8424	-1.3959	J131122.15-012345.6	19.60	X	X	P	X	X	X	15.6 ± 4.1	-1.00	6.98	5
152	197.9071	-1.3304	J131137.68-011950.0	20.42	P	X	X	X	X	X	78.9 ± 12	-0.64	5.97	2,4,8
153	197.9144	-1.3956	J131139.42-012344.1	21.29	P	X	X	X	X	X	5.81 ± 5.46	-1.00	7.29	2,4,7
157	197.9352	-1.3191	J131144.39-011909.3	20.49		X	X	P	X	X	20.1 ± 20.0	-0.52	3.40	2
160	197.9597	-1.4248	none			X	P	X	X	X	13.3 ± 3.5	-0.28	9.19	2,6
162	197.9695	-1.2442	none			X	X	P	X	X	9.16 ± 1.52	-0.35	5.64	1,2,5
163	197.9758	-1.3797	J131154.23-012246.9	19.99	X	P	X	X	X	X	23.3 ± 6.0	-0.60	7.39	1,2,4,8
166	197.9864	-1.2198	J131156.76-011311.8	13.26		P	X	X	X	X	82.1 ± 9.9	-0.92	6.76	2,4,8
167	197.9928	-1.1745	J131158.32-011026.8	16.65		X	P	X	X		6.54 ± 2.72	0.62	9.29	1,5

Significantly variable sources and their SDSS optical counterparts, as described in §2.2.1. Bold indicates the flare described in detail in the text. SDSS positions may differ slightly from X-ray source positions, but are within X-ray positional uncertainty. I_{AB} magnitudes are calculated from SDSS *ugriz* magnitudes using Lupton (2005). Compare to $m^* = 18.5$ from Lemze et al. (2009) for I_{AB} . X marks epochs when the object would be located within the ACIS FOV, regardless of whether it is detected during the epoch. P indicates the epoch of peak count rate, for which the rate, HR and θ are presented. H and S bands are as described in the text.

Flags: (1) High pre-peak uncertainty (2) XMM detected source (3) SDSS flagged as possible QSO (4) SDSS flagged likely star. A small fraction may also be QSOs or other bright, unresolved objects. (5) Possible pre-peak nondetection (6) SDSS object visible but not catalogued (7) Variability pattern inconsistent with flare (8) Pre-existing match in 1RXH (ROSAT Scientific Team 2000) or 2RXP (ROSAT Consortium 2000)